



HAL
open science

From identification to functional characterization of cyriotoxin-1a, an antinociceptive toxin from the spider *Cyriopagopus schioedtei*

Tânia C. Gonçalves, Evelyne Benoit, Michael Kurz, Laetitia Lucarain, Sophie Fouconnier, Stéphanie Combemale, Lucie Jaquillard, Brigitte Schombert, Jean-Marie Chambard, Rachid Boukaiba, et al.

► To cite this version:

Tânia C. Gonçalves, Evelyne Benoit, Michael Kurz, Laetitia Lucarain, Sophie Fouconnier, et al.. From identification to functional characterization of cyriotoxin-1a, an antinociceptive toxin from the spider *Cyriopagopus schioedtei*. *British Journal of Pharmacology*, 2019, 176 (9), pp.1298-1314. 10.1111/bph.14628 . cea-02121632

HAL Id: cea-02121632

<https://cea.hal.science/cea-02121632v1>



Submitted on 20 May 2020

HAL is a multi-disciplinary open access archive for the deposit and dissemination of scientific research documents, whether they are published or not. The documents may come from teaching and research institutions in France or abroad, or from public or private research centers.

L'archive ouverte pluridisciplinaire **HAL**, est destinée au dépôt et à la diffusion de documents scientifiques de niveau recherche, publiés ou non, émanant des établissements d'enseignement et de recherche français ou étrangers, des laboratoires publics ou privés.

RESEARCH PAPER

From identification to functional characterization of cyriotoxin-1a, an antinociceptive toxin from the spider *Cyriopagopus schioedtei*

Tânia C. Gonçalves^{1,2} | Evelyne Benoit^{2,3}  | Michael Kurz⁴ | Laetitia Lucarain¹ | Sophie Fouconnier¹ | Stéphanie Combemale⁵ | Lucie Jaquillard⁵ | Brigitte Schombert¹ | Jean-Marie Chambard¹ | Rachid Boukaiba¹ | Gerhard Hessler⁴ | Andrees Bohme¹ | Laurent Bialy⁴ | Stéphane Hourcade⁶ | Rémy Bérout⁵ | Michel De Waard^{5,7} | Denis Servent²  | Michel Partiseti¹

¹Integrated Drug Discovery—High Content Biology, Sanofi R&D, Vitry-sur-Seine, France

²Service d'Ingénierie Moléculaire des Protéines (SIMOPRO), CEA, Université Paris-Saclay, Gif-sur-Yvette, France

³Institut des Neurosciences Paris-Saclay (Neuro-PSI), UMR CNRS/Université Paris-Sud 9197, Université Paris-Saclay, Gif-sur-Yvette, France

⁴Integrated Drug Discovery—Synthetic Molecular Design, Sanofi R&D, Frankfurt, Germany

⁵Smartox Biotechnology, Saint-Egrève, France

⁶Neuroscience Therapeutic Area, Neurodegeneration Research, Sanofi R&D, Chilly-Mazarin, France

⁷Institut du Thorax, Inserm UMR 1087/CNRS UMR 6291, LabEx "Ion Channels, Science and Therapeutics", Nantes, France

Correspondence

Denis Servent, Service d'Ingénierie Moléculaire des Protéines (SIMOPRO), CEA, Université Paris-Saclay, F-91191 Gif-sur-Yvette, France. Email: denis.servent@cea.fr

Michel Partiseti, Integrated Drug Discovery—High Content Biology, Sanofi R&D, F-94440 Vitry-sur-Seine, France. Email: michel.partiseti@sanofi.com

Funding information

Sanofi Research & Development (Chilly-Mazarin, France), Grant/Award Number: #153114; French Alternative Energies and Atomic Energy Commission (CEA, Gif-sur-Yvette, France); Agence Nationale de la Recherche, Grant/Award Number: ANR-11-LABX-0015

Background and Purpose: The Na_v1.7 channel is highly expressed in dorsal root ganglia of the sensory nervous system and plays a central role in the pain signalling process. We investigated a library prepared from original venoms of 117 different animals to identify new selective inhibitors of this target.

Experimental Approach: We used high throughput screening of a large venom collection using automated patch-clamp experiments on human voltage-gated sodium channel subtypes and then in vitro and in vivo electrophysiological experiments to characterize the active peptides that have been purified, sequenced, and chemically synthesized. Analgesic effects were evaluated in vivo in mice models.

Key Results: We identified cyriotoxin-1a (CyrTx-1a), a novel peptide isolated from *Cyriopagopus schioedtei* spider venom, as a candidate for further characterization. This 33 amino acids toxin belongs to the inhibitor cystine knot structural family and inhibits hNa_v1.1–1.3 and 1.6–1.7 channels in the low nanomolar range, compared to the micromolar range for hNa_v1.4–1.5 and 1.8 channels. CyrTx-1a was 920 times more efficient at inhibiting tetrodotoxin (TTX)-sensitive than TTX-resistant sodium currents recorded from adult mouse dorsal root ganglia neurons and in vivo electrophysiological experiments showed that CyrTx-1a was approximately 170 times less efficient than huwentoxin-IV at altering mouse skeletal neuromuscular excitability properties. CyrTx-1a exhibited an analgesic effect in mice by increasing reaction time in the hot-plate assay.

Conclusions and Implications: The pharmacological profile of CyrTx-1a paves the way for further molecular engineering aimed to optimize the potential antinociceptive properties of this peptide.

Abbreviations: CMAP, compound muscle action potential; CyrTx-1a, cyriotoxin-1a; DRG, dorsal root ganglia; HwTx-IV, huwentoxin-IV; ICK, inhibitor cystine knot; NaSpTx, Na_v channel spider toxin; TTX, tetrodotoxin; TTX-R, resistant to tetrodotoxin; TTX-S, sensitive to tetrodotoxin; U2OS cell line, human bone osteosarcoma epithelial cell line

1 | INTRODUCTION

Sensory neurons express many transmembrane proteins that are therapeutic target candidates for the treatment of pain. In particular, inhibitors of ion channels (such as voltage-gated sodium [Na_v] and calcium [Ca_v] channels, transient receptor potential channels, acid-sensing ion channels, piezo proteins, and ionotropic P2X receptors), as well as potassium channel (K_v) enhancers, are being investigated as potential analgesics (Bennett & Woods, 2014; Waxman & Zamponi, 2014). Na_v channels include nine subtypes (Na_v1.1–1.9), each of them having different functions due to specific expression patterns and/or singular biophysical properties (Catterall, Goldin, & Waxman, 2005; de Lera Ruiz & Kraus, 2015). During this last decade, attention has been given to several Na_v channel subtypes (Na_v1.1, 1.3, and 1.6–1.9) as potential analgesic targets (Cardoso et al., 2017).

Among these Na_v channels, the Na_v1.7 channel seems to be one of the most interesting target to treat chronic debilitating pain (Vetter et al., 2017). Indeed, this subtype is highly expressed in the sensory nervous system, principally in small and large dorsal root ganglia (DRG) neurons, the anatomical support of pain signalling from the skin and organs to the spinal cord (Dib-Hajj, Yang, Black, & Waxman, 2013). Furthermore, a multitude of genetic mutations of the Na_v1.7 protein are linked to painless or painful phenotypes (de Lera Ruiz & Kraus, 2015; Vetter et al., 2017). Moreover, it is well established that low MW compounds that target Na_v channels, such as tetrodotoxin (TTX), attenuate chronic and debilitating pain in humans (Hagen et al., 2017). However, pronounced side effects have been described, such as nausea, dizziness, oral numbness, and tingling, due to a lack of selectivity (Hagen et al., 2017). The current challenge is thus to identify a new therapeutic class of analgesic molecules that blocks the Na_v1.7 channel with high selectivity compared to other Na_v channels, particularly the Na_v1.5 and the Na_v1.6 and 1.4 channels, because of cardiac and neuromuscular safety issues, respectively.

Several peptide toxins from animal venoms (spiders, scorpions, cone snails, sea anemones, centipedes) have been reported to block or modulate Na_v channel function (Israel, Tay, Deuis, & Vetter, 2017). Some of them, mainly isolated from spider venoms, showed promising selectivity for Na_v1.7 channels (Vetter et al., 2017). Their sequence is mostly composed of 30–35 amino acids, including three disulfide bridges with an inhibitor cystine knot (ICK) motif. These positively charged toxins are gating-modifier peptides that bind to the receptor sites 3 (on Domain IV) and/or 4 (on Domain II) of Na_v channels, inducing variable pharmacological effects in in vitro tests and in vivo pain models (Saez et al., 2010). For instance, huwentoxin-IV (HwTx-IV) and the tarantula toxin GpTx-1, two well-characterized Na_v1.7 channel-blocking spider toxins with high selectivity over Na_v1.4 and Na_v1.5 channels, have analgesic properties in animal models. However, they also produce strong side effects such as inactivity, paralysis, and death in standard pain tests in rodents, due to the lack of selectivity over the Na_v1.6 channels (Deuis et al., 2016; Gonçalves, Boukaiba, et al., 2018). Other spider toxins, such as protoxin-II, exhibit a 100-fold higher potency on Na_v1.7, compared with all Na_v channels, except for Na_v1.6 channels. Interestingly, the

in vivo safety margin of this toxin is increased for the mutant peptide JNJ 63955918, due to an improved selectivity against Na_v1.1, 1.2, and 1.6 channels (Flinspach et al., 2017). Very recently, the Jingzhaotoxin-V analogue AM-8145 was reported to display a more than 100-fold higher potency on Na_v1.7 compared to all Na_v channels (Moyer et al., 2018).

The present work reports the identification, structural characterization, and pharmacological profile of the first toxin (CyrTx-1a) isolated from the venom of *Cyriopagopus schioedtei* spider, using a high throughput electrophysiological screening assay on Na_v channels. This ICK toxin is shown to possess nanomolar range affinity for Na_v1.1–1.3, 1.6, and 1.7 channels and micromolar affinity for other channel subtypes and to exhibit analgesic effects in rodent pain models. It represents an interesting lead for new analogues designed to exhibit a better therapeutic window.

2 | METHODS

2.1 | Isolation and purification of CyrTx-1a

A library was prepared from 117 different animal venoms by crude venom fractionation using an analytical RP-HPLC C18 column (XBridge™ BEH 130, 3.5 μm and 4.6 mm ID × 250 mm L column) attached to an Agilent 1260 HPLC (Agilent Technologies). Primary fractions were first evaluated in a functional screening assay on an engineered HEK-293 cell line (RRID:CVCL_0045) overexpressing human (h) Na_v1.7 and hNa_v1.5 channels using the IonWorks Quattro platform (Molecular Devices, USA). For instance, the *C. schioedtei* spider venom, one of the venoms of interest, was separated into fractions that contained between 5 and 15 peptides each at an estimated concentration of 0.5 μg·μl⁻¹. Active fractions were finally subfractionated using cation exchange chromatography with a TOSOH Bioscience column (TSK gel SP-STAT, 7 μm, 4.6 mm ID × 10 cm L, TOSOH Bioscience, Germany) onto an Agilent 1260 HPLC (Agilent Technologies) to individualize the compounds. The purified compounds were screened on HEK-293 cells overexpressing hNa_v1.7, hNa_v1.2, hNa_v1.5, and hNa_v1.6 channels, using the QPatch HTX automated electrophysiology platform (Sophion BioScience, Denmark), leading to the identification of CyrTx-1a as one of the peptides of interest.

2.2 | Amino acid sequencing of CyrTx-1a

The peptide amino acid sequence was determined by de novo MS/MS sequencing and Edman degradation. The purified venom peptide obtained after successive RP-HPLC and cation exchange chromatography, from a starting material of 2 mg, was resuspended in 100 mM ammonium bicarbonate (pH 8), reduced with 17 mM tris(2-carboxyethyl)phosphine hydrochloride (incubated at 55°C for 1 hr) and alkylated with 24 mM iodoacetamide (incubated at room temperature in the dark for 1 hr) prior to enzyme digestion. The reduced/alkylated venom peptide was digested by using trypsin or

V8 proteases. The enzyme was added at a 1:10 ratio (enzyme/peptide, w/w) and incubated overnight at 37°C before LC–MS analyses.

A Waters Q-TOF Xevo G2S mass spectrometer equipped with an Acquity UHPLC system and Lockspray source was used for the acquisition of the LC–ESI–MS and LC–ESI–MS/MS data and the amino acid sequence determination based on Edman degradation was performed using an Applied Biosystems gas-phase sequencer model 492 (s/n: 9510287 J). These protocols are detailed in the Supporting Information.

2.3 | Chemical synthesis and folding of CyrTx-1a

CyrTx-1a was assembled stepwise using 2-chlorotrityl chloride resin (substitution rate of 1.6 mmol·g⁻¹) by solid-phase fmoc chemistry on a Symphony Synthesizer (Protein Technologies Inc.). Amino acid coupling reaction was 15 min (repeated three times to increase the coupling yield). After resin cleavage and deprotection with 92.5% (vol) TFA, 2.5% H₂O, and scavengers (1,3-dimethoxybenzene [2.5%] and triisopropylsilane [2.5%]), the peptide was purified to homogeneity by C18 RP-HPLC on a Jupiter Proteo column (Phenomenex, 4 μm, 21.2 mm ID × 250 mm L) using an Agilent Technologies preparative HPLC (1260 Infinity). Finally, CyrTx-1a was folded/oxidized in 50 mM Tris–HCl, pH 8.3 during 72 hr. The resulting oxidized CyrTx-1a with its three disulfide bridges was purified to homogeneity (>99% purity according to the integration of the purified chromatogram peak at 214 nm) using RP-HPLC with the Jupiter Proteo column. The molecular mass of CyrTx-1a was determined by LC–ESI–QTOF MS. The absence of contaminant masses attested to the purity of synthetic CyrTx-1a.

2.4 | 3D structure of CyrTx-1a

The structure of CyrTx-1a was determined by high-resolution NMR spectroscopy in aqueous solution (10% D₂O) of 6 mg·peptide ml⁻¹ in 50 mM phosphate buffer at pH 5.0 and a temperature of 305°K. Data were obtained on a Bruker Avance 700 MHz using standard 2D spectra. Resonances were assigned with 2D spectra including DQF-COSY, TOCSY, NOESY, ¹H–¹³C-HSQC, and ¹H–¹⁵N-HSQC. For conformational analysis, NOE-based distance restraints were obtained from a NOESY spectrum with 200 ms mixing time. Four hundred thirty-one distance restraints were used in a simulated annealing protocol starting from a linear, extended structure including 71 intra-residual distances, 126 sequential distances, 69 medium distances (two to four amino acids apart), and 165 long range distances (>4 amino acids apart). Calculations were performed with the software package SYBYL version 2.1.1. All energy calculations were based on AMBER7 F99 force field. Distance restraints for non-separated methylene protons and methyl groups were used with pseudoatom correction: 0.9 Å were added to the upper bound for methylene groups, 1.0 Å was added for methyl groups. Twenty structures were obtained which converged well. The rmsd over all backbone atoms was 0.465 ± 0.285 Å.

2.5 | Toxins used for functional assays

Lyophilized synthetic CyrTx-1a (molecular mass of 3578.68, purity rate > 97%), lyophilized synthetic HwTx-IV, molecular mass of 4106.811, purity rate > 97%; Smartox Biotechnology, Saint-Egrève, France), and TTX citrate (molecular mass of 319.27, purity rate > 98%; Sigma-Aldrich, Saint-Quentin Fallavier, France) were dissolved in PBS (1×) solution to give stock solutions of 6.8, 6.1, and 2.85 mM, respectively. Successive dilutions were then performed in the different standard physiological media, prior to experiments.

2.6 | Cell lines used for functional assays

Generation of inducible cell lines was achieved using the Flp-In[®] T-Rex[®] or Jump-In[®] T-Rex[®] expression system (Invitrogen, USA). For this purpose, cDNAs encoding for hNav_v1.5 (NM_000335), hNav_v1.2 (NM_021007.2), hCa_v3.1 (NM_018896.4), and hCa_v3.2 (NM_021098.2) were cloned into the Flp-In[®] T-Rex[®] expression vector and subsequently transfected into HEK-293 or CHO cell line (RRID:CVCL_0213), using the FuGENE[®] transfection reagent (Promega, France). The cDNA encoding for hK_v7.1 (NM_000218.2) was cloned into the Jump-In[®] T-Rex[®] expression vector and subsequently transfected into human bone osteosarcoma epithelial (U2OS) cell line (RRID:CVCL_0042), using the FuGENE[®] transfection reagent. Recombinant HEK-293 cell lines stably overexpressing hNav_v1.7, 1.1, and 1.8 channels were purchased from Eurofins (St. Charles, MO, USA), those for stably overexpressing hNav_v1.6 channels from ChanTest (Cleveland, OH, USA), and those stably overexpressing hNav_v1.3 and 1.4 channels from SB Drug Discovery (UK). Cells overexpressing hNav_v1.7 channels were cultured in suspension in FreestyleTM293 (Gibco, Thermo Fisher Scientific, Villebon-sur-Yvette, France). Those overexpressing hNav_v1.2 and 1.5 channels were cultured in DMEM with GlutaMAX[™] supplement (Gibco), those overexpressing hNav_v1.1, 1.6, and 1.8 channels were cultured in DMEM/F12 with GlutaMAX[™] supplement (Gibco), while those overexpressing hNav_v1.3 and 1.4 channels were cultured in minimum essential medium (Sigma). In-house U2OS-Jump-In-T-REX cells were kept in culture in McCoy's 5A medium with GlutaMAX[™] supplement (Gibco). CHO cells heterologously overexpressing hCa_v1.2/β2/α2δ1 (ChanTest), hCa_v3.1 and hCa_v3.2 channels were cultured in Ham's F12 nutrient mix with GlutaMAX[™] medium (Gibco). Those overexpressing hK_v2.1 channels (ChanTest) were cultured in DMEM/F-12 Glutamax (Gibco), and those overexpressing hK_v11.1 channels (B'SYS GmbH, Switzerland), encoded by the human *ether-a-go-go*-related gene, were cultured in DMEM/F12 nutrient mixture Ham's medium (Sigma). All culture media contained FBS (10%, Gibco) and selected antibiotics and additives, as recommended by the manufacturer. Cells were grown in flasks, under standard conditions (37°C, air supplemented with 5% CO₂), and sub-cultured/passaged every 3 to 4 days using Accutase[®] (Sigma) or TrypLE Select (Gibco) as enzymatic dissociation to detach the cells. At least 12 to 24 hr prior to experiments, doxycycline (BD Biosciences) was added to induce target expression when needed.

2.7 | Animals and primary culture of DRG neurons used for functional assays

All animal care and experimental procedures in this study complied with the guidelines established by the French Council on animal care “Guide for the Care and Use of Laboratory Animals” (EEC86/609 Council Directive—Decree 2001-131), and the experimental protocols were approved on November 27, 2015, by the French General Directorate for Research and Innovation (project APAFIS#2671-2015110915123958v3 authorized to E. B.). Animal studies are reported in compliance with the ARRIVE guidelines (Kilkenny et al., 2010) and with the recommendations made by the *British Journal of Pharmacology*. The experiments were performed using 113 (80 for pain sensitivity assays, 29 for neuromuscular system assay and four for primary cultures of DRG neurons) adult female Swiss mice (*Mus musculus*, 10–12 weeks of age and 28–32 g body weight; catalogue # APB:8115) purchased from Janvier Elevage (Le Genest-Saint-Isle, France). The provider health reports indicated that the animals were free of known viral, bacterial, and parasitic pathogens. The choice of adult Swiss mice was guided by the fact that these outbred animals are more sensitive to morphine than inbred ones (Capasso, Di Giannuario, Loizzo, Pieretti, & Sorrentino, 1994). In addition, taking into account, first, that a clear majority of patients with pain has been reported to be women (Mogil, 2012) and, second, the 3Rs for more ethical use of animals in testing, only female mice were included in our study. The animals were acclimatized for at least 48 hr before experiments at the CEA animal facility. They were housed in a 12-hr light/dark cycle and controlled temperature room, four to a cage containing bedding and a cardboard tube for environmental enrichment and were allowed free access to water and food. This study was experimentally designed to have equal group sizes of at least 10 animals per group for pain sensitivity assays and at least five animals per group for neuromuscular system assay, with intravenous injection as an exclusion criterion. In addition, randomization and blinding (the experimenter being blind to treatment group) were undertaken in all animal experiments.

After anaesthesia, with 2.0–2.5% isoflurane inhalation, and killing, by cervical vertebrae dislocation, the DRG were dissected from intervertebral foramina of the vertebrate column and enzymically dissociated, as reported previously (Gonçalves, Boukaiba, et al., 2018). The neurons were cultured under standard conditions (37°C, 95% air and 5% CO₂) on 12-mm glass coverslips placed in a 24-well plate coated with 100 µg·ml⁻¹ of murin laminin and 10 µg·ml⁻¹ of poly-D-lysine (Sigma-Aldrich). The culture medium was composed of a Neurobasal A medium (Gibco) added with Dulbecco's PBS (1×) without CaCl₂ and MgCl₂ (1.68%; Gibco), BSA (16.83 µg·ml⁻¹; Sigma-Aldrich), corticosterone (214.85 nM; Sigma-Aldrich), T3 hormone (56.06 nM; Sigma-Aldrich), horse serum (5%; Gibco), penicillin/streptomycin (47.64 U·ml⁻¹; Gibco), nerve growth factor (83.33 ng·ml⁻¹; Sigma-Aldrich), N2 supplement (3.18×; Gibco), and L-glutamine (1.90 mM; Sigma-Aldrich). One day later, cytosine β-D-arabino-furanoside (2 µM; Sigma-Aldrich) was added to the medium to inhibit astrocyte proliferation. Experiments were carried out within 2 to 6 days after neuron dissociation.

2.8 | Electrophysiological recordings

Automated and manual patch-clamp recordings were performed on cell lines and DRG neurons as described in the Supporting Information. In vivo recordings from the neuromuscular system of anaesthetized mice were performed by using a minimally invasive electrophysiological method and the Qtrac[®] software (Prof. H. Bostock, Institute of Neurology, London, UK), as detailed previously (Gonçalves, Boukaiba, et al., 2018). By means of a digital-to-analogue converter, this software allowed delivering the stimulation sequences to be performed and, in return, recording (at a sampling frequency of 10 kHz) and analysing the compound muscle action potential (CMAP) collected from the stimulated muscle. After being weighed, a given mouse was placed in an anaesthesia-induction chamber in which a mixture of oxygen (0.4 L·min⁻¹), air (0.2 L·min⁻¹), and isoflurane (AErrane[®], Baxter S.A., Lessines, Belgique; 2.0–2.5%) was diffused. When the mouse was anaesthetised, it was transferred to a heating pad to maintain body temperature throughout the experiments (35.99 ± 0.03°C, as determined in 29 mice using a rectal probe). The animal's muzzle was positioned at the level of a mask where the anaesthetic gas mixture was conveyed to keep the animal anaesthetised. If necessary, the percentage of isoflurane was adjusted to maintain the depth of the anaesthesia. Electrical stimulations were delivered to the caudal motor nerve (at the base of the tail) by two stimulators (A395, World Precision Instruments, Sarasota, FL, USA) via two surface electrodes, and the CMAP was recorded using fine needle electrodes inserted into the tail muscle and connected to an amplifier (Disa EMG 14C13) and then to a hum bug (Quest Scientific). Intramuscular injections (4-µl maximal volume) of PBS solution without (to test for any effect of the vehicle) or with various concentrations of CyrTx-1a or TTX were administered at the base of the tail (between stimulation and ground electrodes) with a 10 µl micro-syringe. The toxin and/or vehicle effects on selected excitability parameters, such as the excitability threshold and CMAP amplitude continuously recorded over time, were assessed by online recordings initiated ≈5 min before a given injection. The duration of CyrTx-1a and TTX effects and the identification of the toxin underlying mechanism(s) of action were investigated by performing five different excitability tests (stimulus–response, strength–duration, and current–threshold relationships, as well as threshold electrotonus and recovery cycle; detailed in Cerles et al., 2017), before and from 30 min to 12 hr after a given injection. More than 30 parameters, providing complementary information on ion channels, receptors, and pumps, as well as on the passive membrane properties of the neuromuscular system (Kiernan & Bostock, 2000; Krishnan, Lin, Park, & Kiernan, 2008), were determined and analysed from these five excitability tests.

2.9 | Heat and tactile pain sensitivity of mice in vivo

Prior to hot-plate testing, each mouse underwent a 30-min acclimation to the experimental laboratory environment (in its home cage). Then, mice were either not injected or received an intraplantar

injection of 5–10 μl of PBS or toxin solution in each hind paw under low anaesthesia achieved by means of isoflurane (AErrane[®], Baxter S.A.) inhalation. After 60 min rest in its home cage, the mouse was put on the hot-plate set at the temperature of $55.0 \pm 0.2^\circ\text{C}$. The measured parameter as the first pain-related manifestation was the latency (in seconds) for the animal either to shake one of its two hind limbs or to jump. This latency, considered as a painful response to heat, was recorded simultaneously by two observers (one being blind to treatment group) with a timer integrated into the set-up. A maximal cut-off time of 30 s was used to prevent tissue damage.

Tactile sensitivity was assessed using an automated plantar von Frey apparatus (Dynamic Plantar Aesthesiometer 37450, Ugo Basile, Comerio, Italy). Prior to testing, each mouse was placed on a mesh grid, surrounded by a clear Plexiglas barrier with a top cover and left to calm down for 30 min without probing. After the settling phase, the mouse was motionless allowing for either of its hind limbs to be touched by a flexible plastic fibre of a fixed diameter. The fibre was pressed through the mesh grid against the plantar surface at a right angle, and the force of application increased slowly (at the determined rate of $1.67 \text{ g}\cdot\text{s}^{-1}$). The force intensity (in g) at which the animal removed its hind limb was recorded with a timer integrated into the set-up as the mean of at least four tests. A cut-off automatically occurred if the animal did not remove its hind limb when the point at which the greatest pre-set force was met, to prevent tissue damage. The force intensity was determined every 5 min during 30–45 min before and 15 min after intraplantar injection of 5 μl of PBS or toxin solution in each hind limb, under mild anaesthesia with isoflurane.

2.10 | Data and statistical analyses

The data and statistical analysis comply with the recommendations of the *British Journal of Pharmacology* on experimental design and analysis in pharmacology. Sigmoid nonlinear regressions through data points (correlation coefficient = r^2) were used to calculate theoretical concentration–response curves, according to the Hill equation (GraphPad Prism version 5 [RRID:SCR_002798] or QPatch assay software): $Rt/Rc = 1/[1 + ([\text{toxin}]/IC_{50})^{n_H}]$, where Rt/Rc is the response recorded in the presence of a given toxin (Rt) and expressed as percentage of the value obtained in absence of toxin (Rc), $[\text{toxin}]$ is the toxin concentration, IC_{50} is the toxin concentration necessary to inhibit 50% of the response, and n_H is the Hill number. The conductance (g) was calculated from the peak current amplitude (I) according to the following equation: $g = I/(V_T - V_{Na})$, where V_T is the test-pulse voltage and V_{Na} is the equilibrium potential of Na ions. The Boltzmann equation (GraphPad Prism version 5 software) was used to calculate the theoretical conductance–voltage curves corresponding to data point fit: $g/g_{\text{max}} = 1 - [1/(1 + \exp((V_T - V_{T50\%})/k_g))]$, where g/g_{max} is the conductance expressed as percentage of the maximal conductance (g_{max}) calculated at strongly positive test-pulses, $V_{T50\%}$ is the test-pulse voltage corresponding to 50% maximal conductance, and k_g is the slope of the curve. The Boltzmann equation was also used to calculate the theoretical steady-state inactivation–voltage curves corresponding to data point fit: $I/I_{\text{max}} = 1/[1 + \exp((V_P - V_{P50\%})/k_h)]$,

where I/I_{max} is the peak current amplitude expressed as percentage of the maximal amplitude (I_{max}) recorded in response to strongly negative pre-pulses (V_P), $V_{P50\%}$ is the pre-pulse voltage corresponding to 50% maximal peak amplitude of current, and k_h is the slope of the curve. The evaluation of current kinetics was performed by calculating the time to peak (t_p) and the time constant of the current inactivation (τ_h). The time to peak was defined as the time between test-pulse triggering and the peak current, and the time constant of the current inactivation was calculated according to the following equation, assuming a mono-exponential decay as a function of time: $I(t) = I_{(0)} e^{(-t/\tau_h)}$.

Data are expressed as means \pm SDs of n different experimental biological samples. The statistical comparison of values was carried out using (a) the parametric two-tailed Student's t test (either paired samples for comparison within a single population or unpaired samples for comparison between two independent populations) or (b) the one-way ANOVA (for comparison between the means of three or more independent populations) followed, if F was significant and if no variance inhomogeneity occurred, by post hoc pairwise t tests with Bonferroni correction. Differences were considered to be statistically significant at $P < 0.05$.

2.11 | Nomenclature of targets and ligands

Key protein targets and ligands in this article are hyperlinked to corresponding entries in <http://www.guidetopharmacology.org/>, the common portal for data from the IUPHAR/BPS Guide to PHARMACOLOGY (Harding et al., 2018), and are permanently archived in the Concise Guide to PHARMACOLOGY 2017/18 (Alexander et al., 2017).

3 | RESULTS

3.1 | Isolation, purification, and de novo amino acid sequencing of CyrTx-1a

A primary high throughput screening of the Smartox venom collection was performed on automated patch-clamp Ionworks Quattro platform using HEK-293 cells overexpressing hNa_v1.7 channels (Figure 1a). Following successful priming and sealing steps, a 10-pulse train protocol from -120 to -10 mV at 10 Hz was elicited, bringing hNa_v1.7 channels from closed to open configuration (Figure 1b,c). The so-called pre-scan performed in the presence of extracellular buffer was used as a control signal. An average peak current from pulse 1 of 880 ± 280 pA ($n = 29$ plates) was elicited. A similar average amplitude was measured from pulse 10 on the same recording (no current run-down was observed under our conditions). In control experiments using the same protocol, no inhibitory effect of 0.1% BSA was found. Conversely, addition of 1 μM TTX produced a full block of the elicited currents ($n = 928$ wells from 29 plates). This expected pharmacology was used as the internal positive control (data not shown).

As mentioned in Figure 1, a total of 7,548 fractions coming from 117 crude venoms were tested from a large variety of species including snake, spider, scorpion, wasp, bee, amphibians, lizard, and fish (see

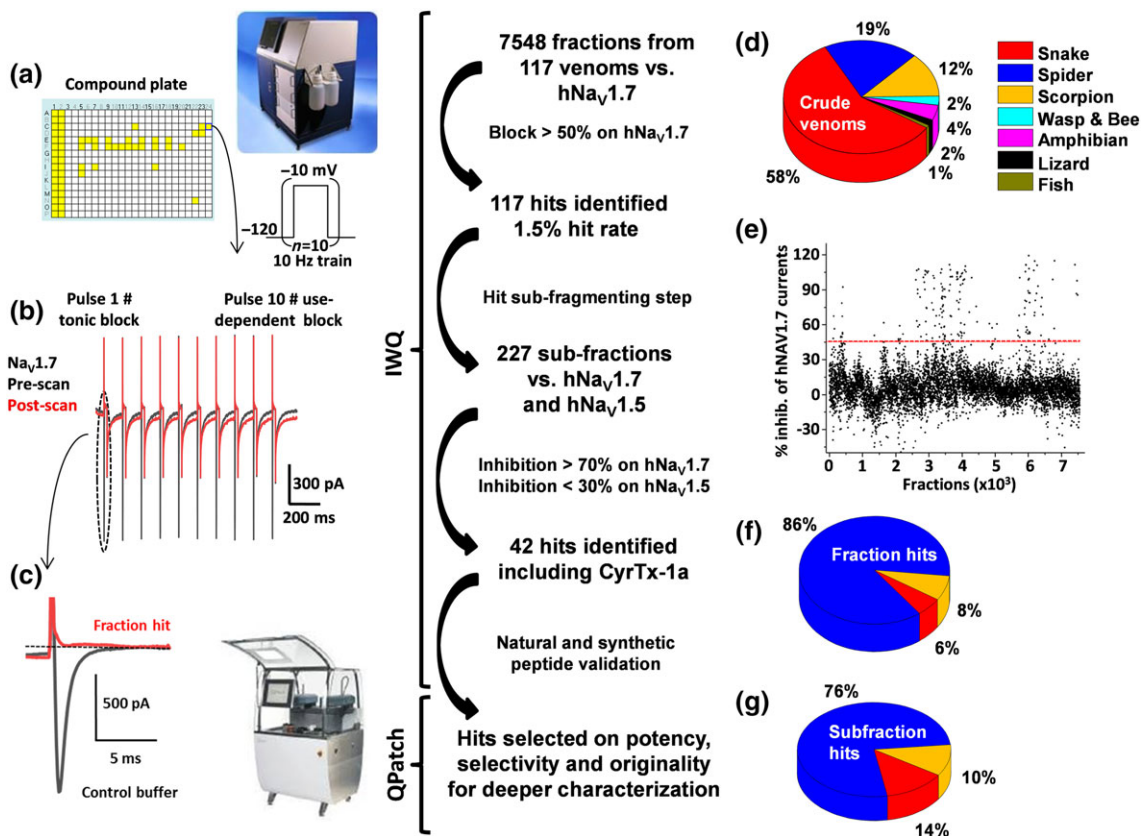


FIGURE 1 Screening flowchart from crude venom fraction to isolated peptide identification. (a) The collection of 117 venoms was prepared into 7,548 fractions individually added to 384-well plates (Columns 1 and 2 are 1 μM TTX full block and Columns 3 and 4 are maximal current obtained in extracellular buffer) for testing versus hNav_v1.7 channels on the Ionworks Quattro (IWQ, Molecular Devices). The train protocol described as an insert was applied before and after 10-min incubation of cells with the fraction containing the toxin of interest. Traces of pre- and post-scan are shown in full (b). Also, tonic block obtained on hNav_v1.7 channels has been enlarged (c). Source of the screened crude venom is shown in (d). Percentage of inhibition for all tested fractions was plotted. As shown in (e), a threshold was set at 50% block (red line). From the venom library tested, only 8% hits on the hNav_v1.7 channels came from scorpion venom, 6% from snake while the majority (86%) was derived from spider venoms (f). (g) Hits were sub-fractioned and tested against hNav_v1.7 and hNav_v1.5 channels to identify most promising hits to be further characterized using whole-cell automated patch-clamp assays (QPatch)

Figure 1d). The 384-well screening plates were prepared in such a way that individual fractions were tested at an average concentration of 0.5 $\mu\text{g}\cdot\mu\text{l}^{-1}$ (500 ng of dry mass suspended in water). An overview of the percentage of inhibition obtained for each fraction before and after application is given in Figure 1e. Note that 97 fractions were discarded because of a negative impact on the sealing process or because they disrupted seals over time. Also, 26 samples which elicited large sodium current increases were removed from the analysis. From the primary screening, 117 fractions were flagged based on their potency versus recombinant Na_v1.7 channels, then selected for sub-fractionation and compound isolation using cation exchange chromatography (Figure 1f). Following this process, 227 sub-fractions from three species (snake, spider, and scorpion; Figure 1g) were prepared and used at a final estimated amount of 100 ng per well. These sub-fractions were tested in our functional automated patch-clamp assays with hNav_v1.7, but also hNav_v1.5 channels (in conventional closed to open configuration protocols), as a first-line selectivity assay. From the 42 hits highlighted at this stage, 14 were discarded because of strong effects on hNav_v1.5 channels.

Figure 2a,b illustrates the screening process for the spider venom *C. schoiedtei* from primary fraction selection to individual purified compound selection by secondary screening. Using the IonWorks Quattro automated patch-clamp system, a peptide was selected for its potent blocking effect on hNav_v1.7 channels at 2.8 μM ($98.9 \pm 1.2\%$ block, $n = 6$ wells from three plates) while fully sparing hNav_v1.5 channels ($4.1 \pm 1.2\%$ inhibition, $n = 6$ wells from three plates; Figure 2b). Following selection through the multi-step chromatographic approach, a new peptide was identified using combined orthogonal reversed-phase and ion exchange techniques (Figure 2c,d). The molecular mass value of 3578.68 Da for this peptide, as determined by LC-ESI-QTOF MS, indicates that the peptide should be amenable to chemical synthesis (inset in Figure 2d).

As this peptide belongs to a species that has not been genotyped, its sequence was determined by de novo sequencing using MS analyses. Hence, the purified peptide was reduced using tris(2-carboxyethyl) phosphine hydrochloride and alkylated with iodoacetamide. The alterations in molecular mass from 3578.7 to 3926.7 Da indicate that the peptide should contain six cysteine residues and hence three

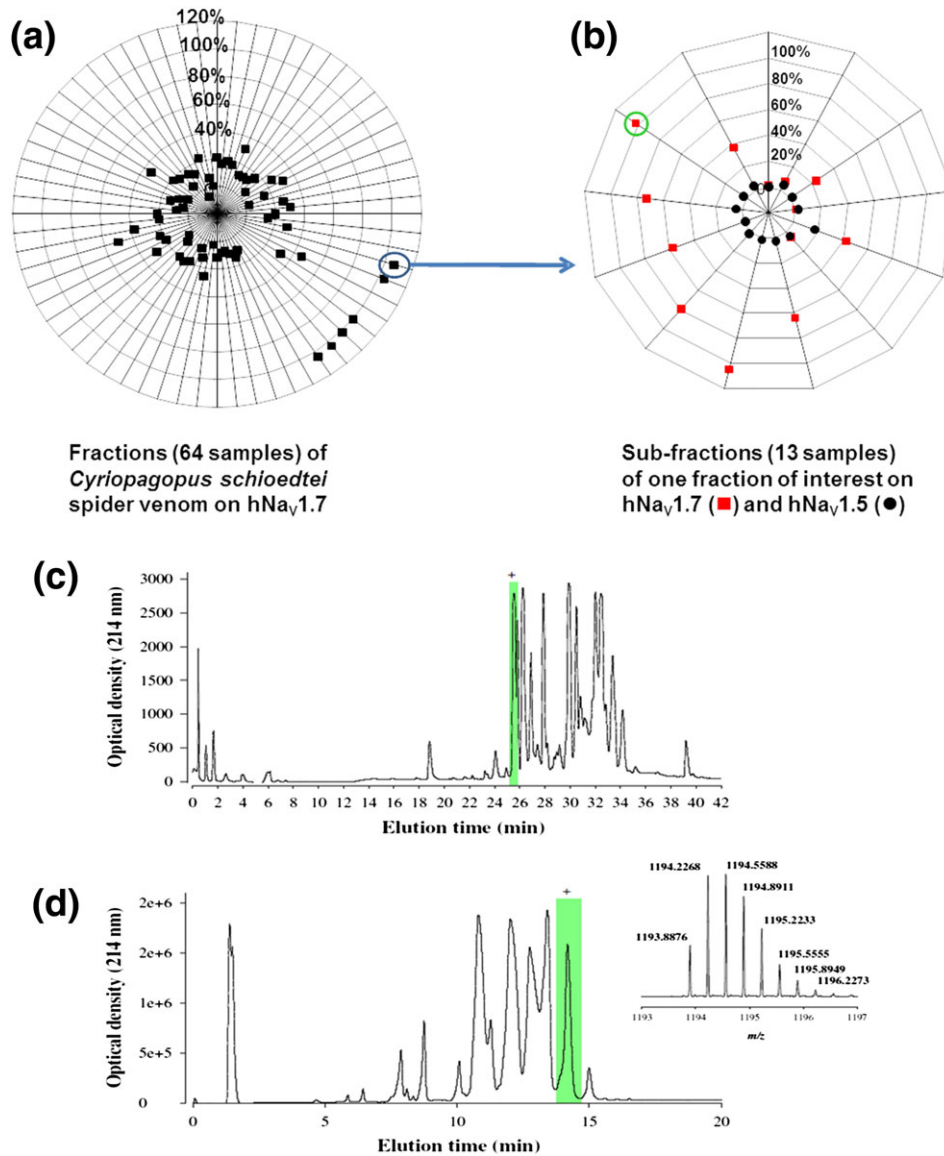


FIGURE 2 Flowchart for hNa_v1.7 channel hit peptide identification. (a) Percentage of inhibition of peak hNa_v1.7 elicited current by application of 0.05 μg of each of the 64 fractions obtained from *Cyriopagopus schioedtei* spider venom. (b) Each fraction of interest was then separated again to isolate one peptide per well. Sub-fractions were tested again in our automated patch-clamp Quattro assay. At this stage, inhibition of hNa_v1.7 and hNa_v1.5 channels was investigated. (c) Fractionation of the crude venom from *C. schioedtei* by reversed-phase chromatography and detection by UV at 214 nm. The fraction containing the peptide of interest is highlighted in green. (d) Cation exchange sub-fractionation of the primary fraction highlighted in (c). The inset illustrates the MS of m/z 1193.8947 [M + 3H]³⁺

disulfide bridges if one takes into account the loss of 1 Da upon reduction of disulfide bridges and the addition of 57.02 Da upon alkylation on each cysteine residue. Samples of the reduced/alkylated toxin were then digested overnight with either trypsin or V8 proteases. The digests were next analysed by LC-ESI-MS(/MS) for de novo sequencing. Table S1 provides the list of fragments detected and sequenced after trypsin and Glu-C digestion. While full sequence coverage of the toxin was obtained by MS, a complementary characterization was performed using Edman degradation, especially for the precise determination of the isobaric leucine and isoleucine residues. The final sequence is reported in Figure 3a with a single post-translational modification identified as C-terminal amidation of the peptide.

The peptide, composed of 33 amino acids (3578.68 Da), was identified as μ-theraphotoxin-Cs1a or cyriotoxin-1a (CyrTx-1a). It is the first toxin described so far from the crude venom of *C. schioedtei* spider, known as the Malaysian earth tiger tarantula, classified in the Ornithoctoninae subfamily. CyrTx-1a contains the ICK architectural motif previously reported in toxins from the same theraphosid spider family, the Na_v channel spider toxin (NaSpTx) family 1 (Figure 3b). Furthermore, comparison of amino acid sequences between CyrTx-1a and the nine most similar toxins (of 33–35 amino acids) with analgesic properties from the NaSpTx family 1 revealed that the peptide shares 82% of identity with hainantoxin-I and μ-theraphotoxin-Hhn2b, and 73% of identity with hainantoxin-III and μ-theraphotoxin-Hhn2a

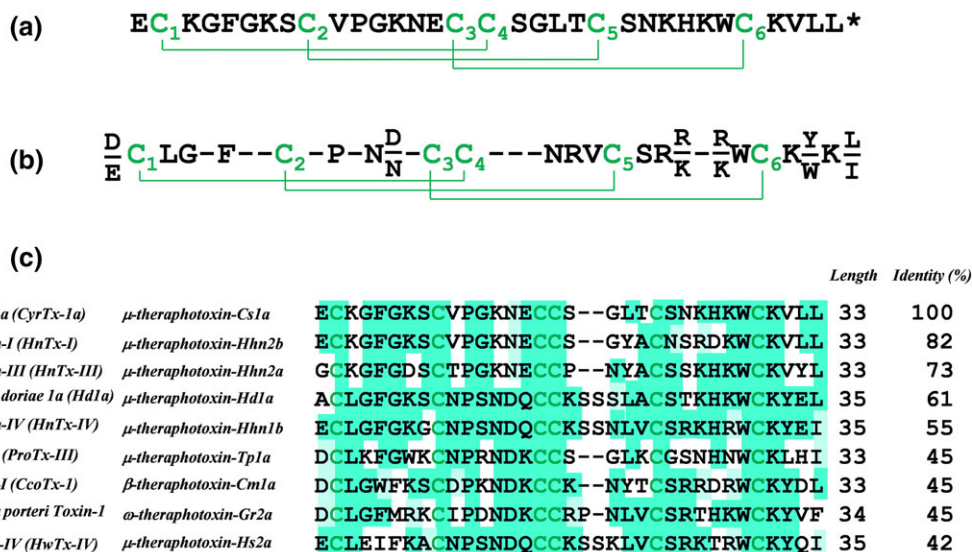


FIGURE 3 Primary structure, disulfide bridge alignment, and sequence homologies of CyrTx-1a. (a) Primary structure of CyrTx-1a. Asterisk denotes amidation. Disulfide bridging, as defined by homology, occurs according to the C1–C4, C2–C5, and C3–C6 pattern. (b) Consensus sequence of the NaSpTx family 1, adapted from Klint et al. (2012). (c) Comparison of amino acid sequences between CyrTx-1a and the nine most similar analgesic toxins from NaSpTx family 1. Sequence alignment performed with Clustal Omega (version 1.2.4 from Emboss programs, EBlosum62 matrix for two pair alignment). The green shading highlights the percentage of identity (Jalview program according to EBlosum62 matrix)

(Figure 3c). In contrast, the well-known potent analgesic peptides ω -theraphotoxin-Gr2a (GpTx-1) and μ -theraphotoxin-Hh2a (HwTx-IV) share only 45% and 42% of identity, respectively, with CyrTx-1a.

3.2 | Chemical synthesis and in vitro folding of CyrTx-1a

CyrTx-1a was chemically synthesized using solid-phase Fmoc chemistry. Figure S1a,b illustrates the HPLC profiles of the crude and purified synthesized peptide, respectively. MS data established that the purified reduced peptide had the expected mass with m/z value of 1195.9097 $[M + 3H]^{3+}$. Finally, the reduced CyrTx-1a peptide was oxidized to produce oxidized/folded CyrTx-1a along with its three disulfide bridges (Figure S1c). The yield of oxidation was 13%, indicating good formation of the secondary structures and easy disulfide bridge connectivity during oxidation. The experimental molecular mass of the synthetic peptide (inset in Figure S1c, 1193.8956 $[M + 3H]^{3+}$) was in close agreement with the theoretical mass (1193.8918). To confirm that the synthetic CyrTx-1a was indeed identical to its native counterpart, both peptides were mixed at equal concentrations and run simultaneously onto analytical RP-HPLC. As a single major peak was detected, we conclude that the two peptides co-elute, hence demonstrating identical retention times on the C18 column (Figure S1d).

3.3 | 3D structure of CyrTx-1a

The 3D solution structure of CyrTx-1a was determined by 2D homonuclear $^1\text{H-NMR}$ spectroscopy. Spectra were recorded at 305°K where the amide resonances show a good dispersion. One signal set of sharp and well-dispersed resonances is indicative of a single

structure in solution (Figure 4a). NMR-derived interproton distances were used for structure calculations with a molecular dynamic-based protocol. An ensemble of 20 conformations was obtained, containing a well-determined backbone conformation of an ICK motif (Figure 4b; PDB: 6GFT). The ^1H -chemical shifts of CyrTx-1a in $\text{H}_2\text{O}/\text{D}_2\text{O}$ highlight the high precision and stereochemical quality of the ensemble of CyrTx-1a structures (Table S2). The entire structure has an electrical dipole moment with a larger positive pole, likely to be important for CyrTx-1a binding to Na_v channels (Figure 4c). Such a motif has also been found for other $\text{Na}_v1.7$ channel inhibitory peptides such as HnTx-IV, ProTx-III, and HwTx-IV (Figure 4d).

3.4 | Effects of CyrTx-1a on hNa_v , hCa_v , hK_v , and hKir channels overexpressed in cell lines

Whole-cell automated patch-clamp (QPatch HTX) experiments performed on HEK-293 cells overexpressing $\text{hNa}_v1.1$ –1.8 channels revealed that 1 μM of synthetic CyrTx-1a was effective to block $\text{hNa}_v1.1$ –1.2–1.3–1.6–1.7 currents while $\text{hNa}_v1.4$ –1.5–1.8 currents were unaffected (Figure 5a). The following increasing order for IC_{50} values was obtained from the concentration–response curves of CyrTx-1a effects on currents flowing through the different channels (Figure 5b): $\text{hNa}_v1.1$ (72.0 ± 10.0 nM, $n = 5$) \approx $\text{hNa}_v1.2$ (75.5 ± 4.3 nM, $n = 8$) \approx $\text{hNa}_v1.6$ (115.0 ± 7.5 nM, $n = 5$) \approx $\text{hNa}_v1.7$ (129.5 ± 2.1 nM, $n = 7$) $>$ $\text{hNa}_v1.3$ (306.6 ± 15.2 nM, $n = 8$) $>>$ $\text{hNa}_v1.4$ (7.7 ± 0.2 μM , $n = 7$) for TTX-sensitive (TTX-S) subtypes, and $\text{hNa}_v1.5$ (>10 μM , $n = 5$) = $\text{hNa}_v1.8$ (>10 μM , $n = 8$) for TTX-resistant (TTX-R) subtypes. Additionally, the peptide had very low affinity for $\text{hCa}_v1.2$, 3.1 and 3.2 and $\text{hK}_v7.1$ and 11.1 and $\text{hKir}2.1$ channels overexpressed in CHO, HEK-293, and U2OS cells, since 10 μM of toxin had no marked effect on currents flowing through these six channels (Figure S2).

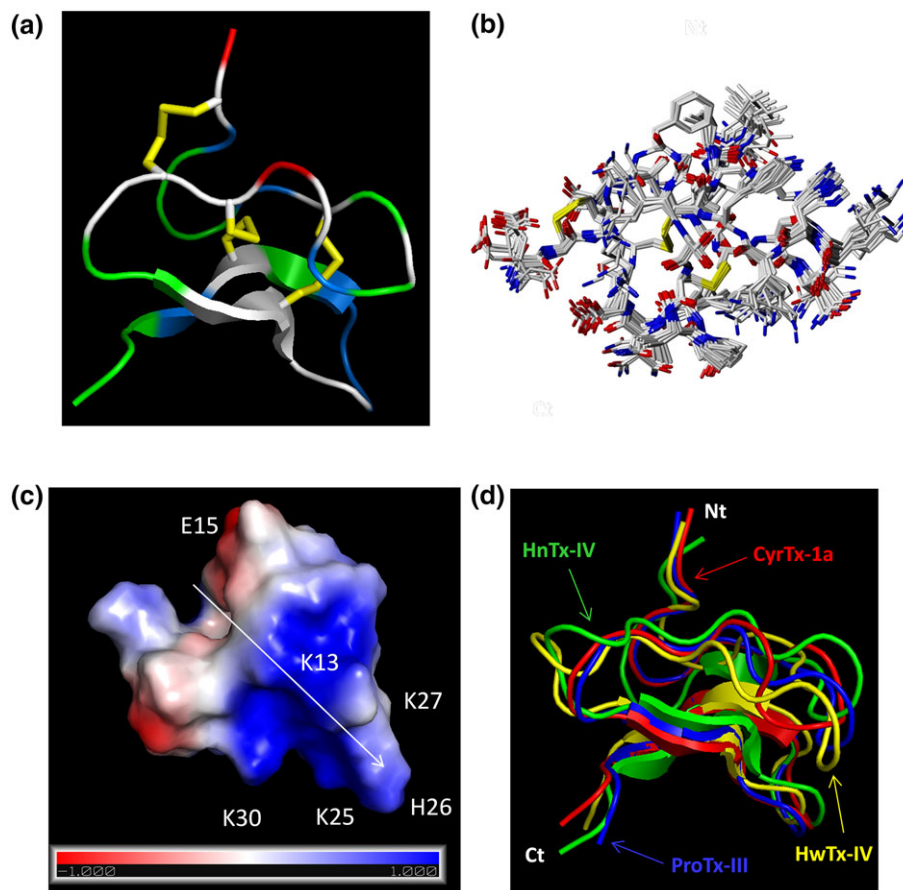


FIGURE 4 Representation of CyrTx-1a identified by PyMOL. (a) Representation of the backbone peptide folding of CyrTx-1a determined by ^1H 2D NMR method. The structure topology is composed of double stranded antiparallel β sheet. The three disulfide bonds are C2–C17, C9–C22, and C16–C29 (in yellow). Hydrophobic residues are coloured in green, and basic and acidic residues are coloured in blue and red, respectively. The other polar residues are coloured in white. (b) Superposition of 20 structures derived from a 6-ns restrained MD simulation (all heavy atoms are shown). All backbone atoms of residues two to 31 were used for fitting. Structures were sampled in 300 ps intervals and energy minimized. The rmsd over all backbone atoms (including residues one to 33) is 0.465 Å with an SD of 0.157 Å. Considering all heavy atoms, the rmsd is 1.072 Å with an SD of 0.285 Å (PDB: 6GFT). (c) Electrostatic charged surface representation of CyrTx-1a. The molecule is rendered as a surface coloured according to the electrostatic potential. As indicated in the coloured legend, an excess of negative and positive charges near the surface are represented in red (–1,000) and blue (1,000), respectively, while fairly neutral potentials are represented in white. The entire structure has a clear dipole potential with E1 and E15 forming a negative zone while K3, K7, K13, K25, H26, K27, and K30 form a positive zone. (d) Superposition of backbone peptide folding of CyrTx-1a and three other toxins of the NaSpTx family 1 previously described to possess analgesic effects (PDB entries of HnTx-IV: 1NIY, ProTx-III: 2MXM, and HwTx-IV: 1MB6)

Further investigation, using whole-cell manual patch-clamp, provided IC_{50} values of 52.7 nM from the concentration–response curves of CyrTx-1a effects on currents flowing through $\text{hNav}_{1.7}$ channels overexpressed in HEK-293 cells (Figure 6a,b). This CyrTx-1a-induced blocking action occurred without any change in steady-state inactivation- and conductance-voltage relationships of $\text{hNav}_{1.7}$ channels (Figure 6c and Table S3).

3.5 | Effects of CyrTx-1a and TTX on adult mouse DRG neurons

Before evaluating the effects of CyrTx-1a on the sodium currents of DRG neurons, the sensitivity of these currents to 100 nM TTX was first determined. Under this condition, two types of neurons were

recorded. The first type (76%, i.e., 16/21 neurons) had only TTX-S current, which was blocked by the toxin to $4.5 \pm 3.0\%$ of initial peak amplitude values within 1 min. The effects of CyrTx-1a (from 0.02 to 1 μM) on these neurons were evaluated by expressing the current peak amplitude recorded in the presence of the peptide relatively to its initial value determined after washing-out TTX with a toxin-free solution for 8–10 min. The second type of neurons (24%, i.e., 5/21 neurons) had a mixed TTX-S and TTX-R current, which was decreased by the toxin to around 55% of initial peak amplitude values. The effects of CyrTx-1a (from 5 to 20 μM) on these neurons were evaluated by expressing the current peak amplitude recorded in the presence of the peptide relatively to its initial value determined in the presence of 100 nM TTX. It is worth noting that relatively large neurons (of more than 25-pF membrane capacitance) were patched, which explains the high percent of TTX-S and low percent of TTX-R

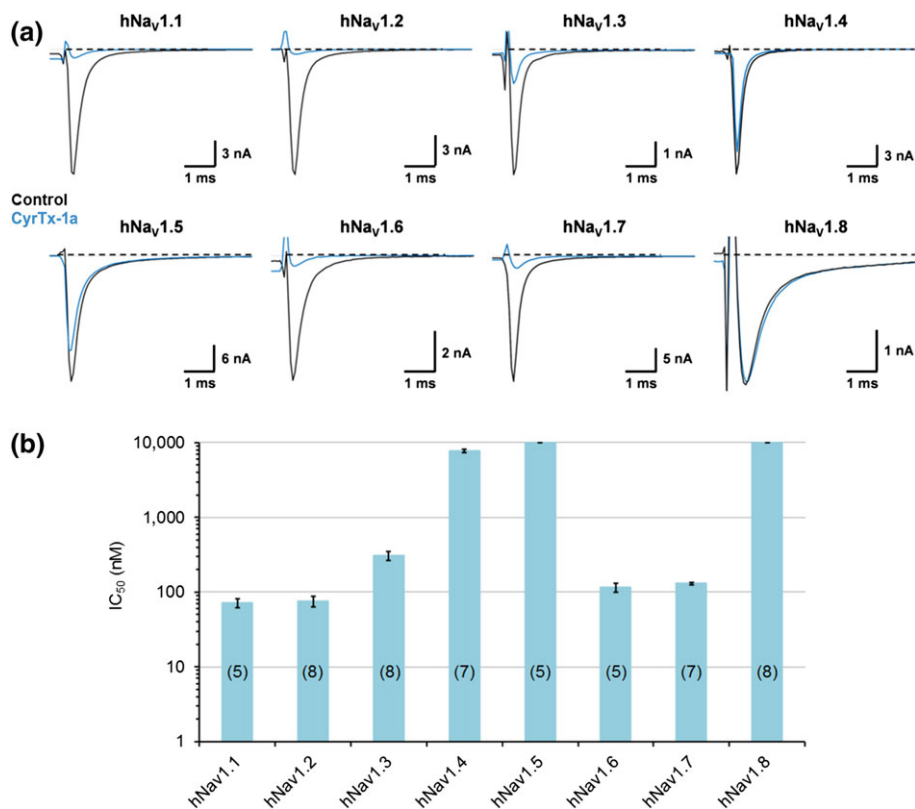


FIGURE 5 Effects of CyrTx-1a on HEK-293 cells overexpressing hNav_v1.1–1.8 channels, using whole-cell automated patch-clamp. (a) Representative traces of sodium currents flowing through hNav_v1.1–1.8 channels, recorded before (control) and after exposure to 1 μM CyrTx-1a. (b) Histograms of IC₅₀ values obtained from the concentration–response curves of CyrTx-1a effects on HEK-293 cells overexpressing hNav_v1.1–1.8 channels. Each value represents the mean ± SD of data obtained from *n* cells (numbers in parentheses). Mean value ± SD of *n_H* was 1.0 ± 0.3

cell recordings. However, the membrane capacitance of neurons having TTX-S current was statistically smaller than that of neurons having TTX-R current, that is, 24.9 ± 8.7 pF (*n* = 16) and 31.9 ± 7.9 pF (*n* = 5), respectively.

Exposing neurons to standard physiological solutions containing various CyrTx-1a concentrations, using a fast solution application system, produced a decrease of sodium current amplitude (Figure 6d) which was dependent on peptide concentration and duration of exposure and on the current sensitivity to TTX. In particular, the concentration–response curves of CyrTx-1a effects on the peak amplitude of TTX-S and TTX-R currents revealed IC₅₀ values of 0.17 and 156 μM, respectively (Figure 6e). The peptide was thus approximately 920 times more efficient to inhibit TTX-S than TTX-R sodium currents of adult mouse DRG neurons. The blocking effects of CyrTx-1a on the peak amplitude of TTX-S current were stationary 5 and 1.5 min after the application of 0.02 and 1 μM of peptide, respectively. Those on the peak amplitude of the TTX-R current were stationary 4 min after the application of 20 μM of peptide. The CyrTx-1a effects on the TTX-R current, not very noticeable, were not further studied, in contrast to those on the TTX-S current.

The peak amplitude of TTX-S current, which was 6 ± 2% of initial values after exposure to 1 μM CyrTx-1a returned to 32 ± 5% of initial values (*n* = 5) by exposing neurons to a peptide-free solution

for 12–15 min, indicating that the effect of CyrTx-1a was, at least, partly reversible. The analyses of activation and inactivation kinetics of TTX-S sodium current in the absence and in the presence of 0.25 and 0.5 μM CyrTx-1a showed that the peptide did not affect these kinetics, as the time to peak (*t_p*) and the time constant of the current decay (*τ_h*) were not significantly modified (Table S4). Similarly, CyrTx-1a (0.25–0.5 μM) did not produce any alteration of steady-state inactivation- and conductance-voltage relationships for neurons exhibiting TTX-S current (Figure 6f and Table S3).

3.6 | Effects of CyrTx-1a on tactile and heat sensitivity of mice in vivo—Comparison with HwTx-IV

Tactile and heat sensitivity testing in mice was performed by intraplantar injection of 102 nmol·kg⁻¹ of CyrTx-1a or 49 nmol·kg⁻¹ of HwTx-IV. A first attempt to evaluate the antinociceptive effect of the two toxins was made using an automated von Frey assay. Tactile sensitivity testing showed that the force intensity at which the mice, injected with 102 nmol·kg⁻¹ of CyrTx-1a or 49 nmol·kg⁻¹ of HwTx-IV, removed their hind limb in response to fibre pressure, that is, 8.6 ± 1.1 g (*n* = 8) and 8.5 ± 1.4 g (*n* = 8), respectively, had tendency (*P* < 0.17) to increase compared to animals injected with PBS, that is,

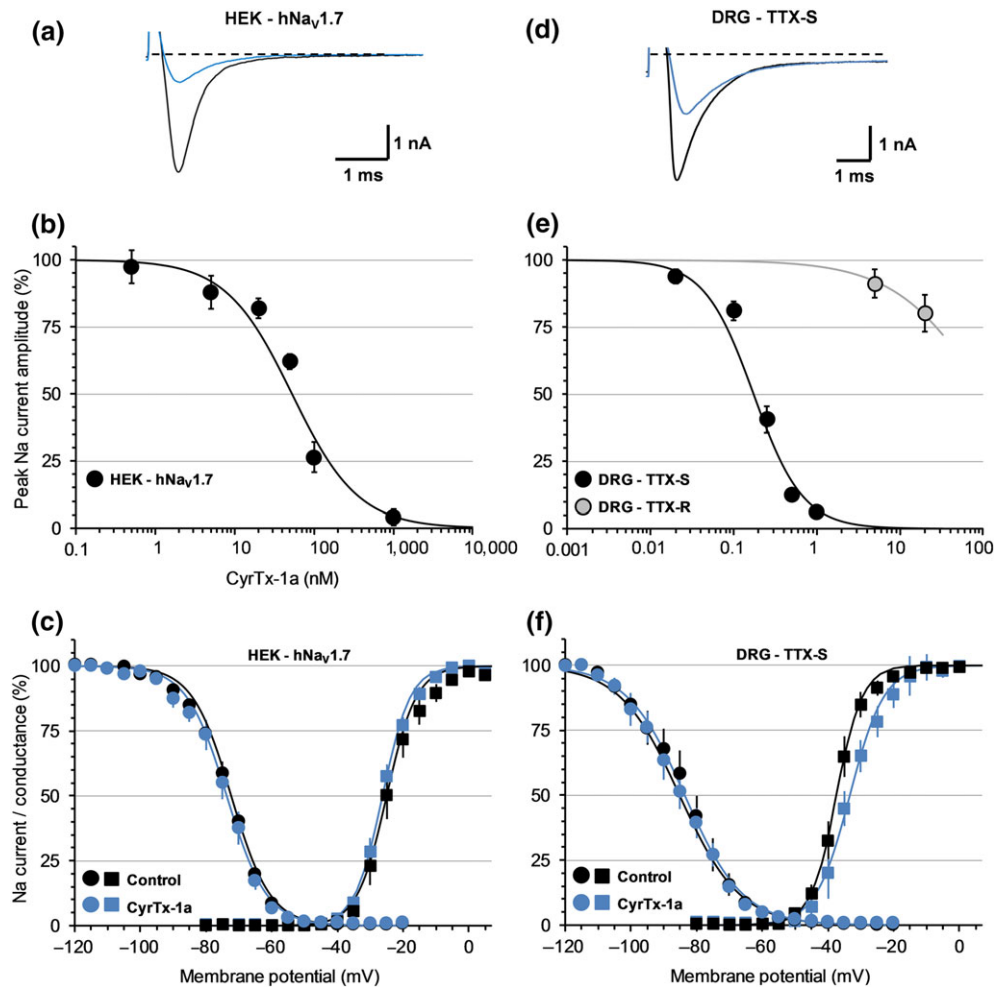


FIGURE 6 Effects of CyrTx-1a on HEK-293 cells overexpressing hNa_v1.7 channels (a–c) and on TTX-S and TTX-R sodium currents of adult mouse DRG neurons (d–f), using whole-cell manual patch-clamp. Representative traces of sodium currents flowing through hNa_v1.7 channels (a) and of TTX-S sodium currents of DRG neurons (d), recorded before (black) and after (blue) exposure to 100 and 250 nM CyrTx-1a, respectively. Concentration–response curves of CyrTx-1a effects on hNa_v1.7 channel current (b) and on TTX-S and TTX-R sodium currents of DRG neurons (e). Each value, expressed as percentage of that obtained before toxin application, represents the mean ± SD of data obtained from five HEK-293 cells and five DRG neurons from four different cell cultures. IC₅₀ and n_H values were, respectively, 52.7 nM and 1.0 for hNa_v1.7 current ($r^2 = 0.954$), 0.17 μM and 1.5 for TTX-S current ($r^2 = 0.961$), and 156 μM and 0.7 for TTX-R current ($r^2 = 1.000$). Steady-state inactivation- (circles) and conductance- (squares) voltage relationships for HEK-293 cells overexpressing hNa_v1.7 channels (c) and for neurons having TTX-S current (f), before and after exposure to 50 nM and 0.25–0.5 μM CyrTx-1a, respectively. Each value represents the mean ± SD of data obtained from five HEK-293 cells and eight DRG neurons from four different cell cultures and is expressed as percentage of either maximal peak amplitude of current at strongly negative pre-pulse voltages or maximal conductance calculated at strongly positive test voltages. The theoretical curves correspond to data point fits with the mean $V_{P50\%}$, k_{1h} , $V_{T50\%}$, and k_g values indicated in Table S3

7.0 ± 1.7 g ($n = 19$; Figure 7a). However, these effects were not significant. Thus, the antinociceptive effect of the two toxins was further investigated using a hot-plate assay. A significant increase in the treated-mouse reaction time to heat, that is, the latency either to shake one of the two hind limbs or to jump, was observed compared to animals injected with PBS (Figure 7b). In particular, the reaction time was increased by 1.83 times for mice injected with CyrTx-1a (17.2 ± 1.7 s, $n = 13$) and by 1.64 times for animals injected with HwTx-IV (15.4 ± 1.9 s, $n = 13$), compared with animals injected with PBS (9.4 ± 0.6 s, $n = 12$). The injection itself did not have any effects as there was no difference in the reaction time or force intensity between mice injected with PBS and non-injected animals (Figure 7).

3.7 | Effects of CyrTx-1a, compared to HwTx-IV, on the mouse neuromuscular system in vivo

Online recordings revealed that the major effect of intramuscular injections of PBS solutions containing various concentrations of either CyrTx-1a (from 0.3 to 448.7 nmol·kg⁻¹ mouse) or HwTx-IV (from 4.1 pmol·kg⁻¹ to 41.4 nmol·kg⁻¹ mouse) to anesthetized mice was a marked decrease of CMAP amplitude. This is exemplified in Figure 8 a for CMAP recordings performed before and between 10 and 15 min after injections of 29.4 nmol kg⁻¹ of CyrTx-1a and 41.4 nmol kg⁻¹ of HwTx-IV. The maximal CMAP amplitude measured 30 min after injections of PBS solution alone, and compared to values before

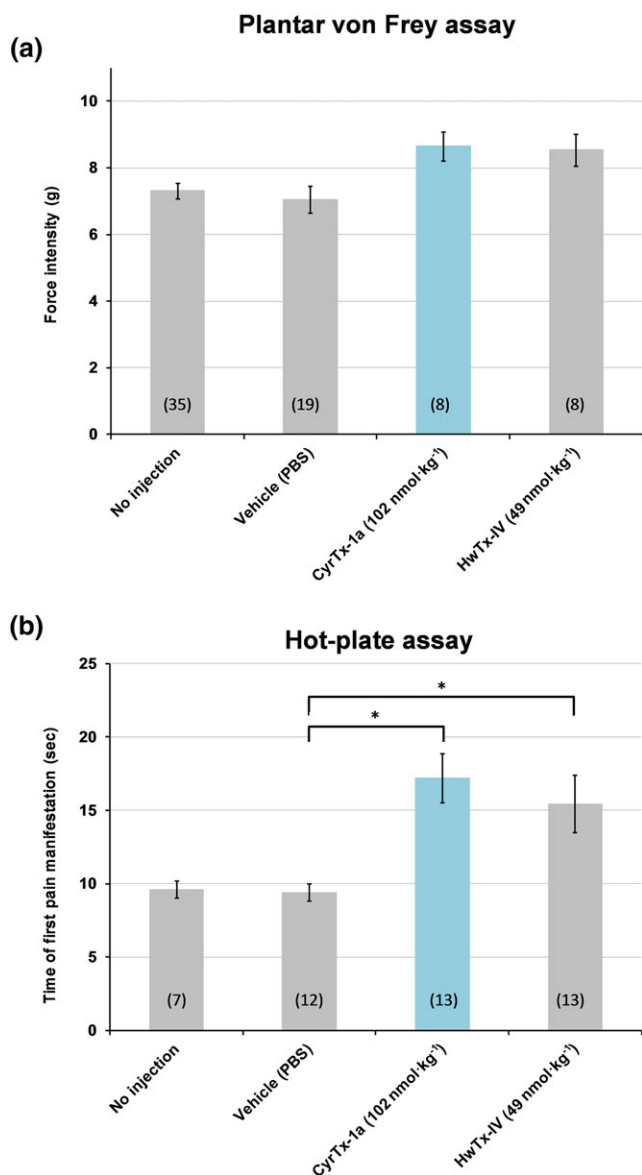


FIGURE 7 Effects of CyrTx-1a on tactile and heat sensitivity of mice in vivo. (a) The tactile sensitivity of mice was assessed using an automated plantar von Frey apparatus, by determining the force intensity at which the animals removed their hind limb submitted to an increasing fibre pressure. The same mice were tested before (no injection) and 15 min after intraplantar injection in each hind limb of 5 μ l of PBS, CyrTx-1a (i.e., 102 nmol·kg⁻¹) or HwTx-IV (i.e., 49 nmol·kg⁻¹). (b) The heat sensitivity of mice was assessed using a hot-plate set at 55.0 \pm 0.2°C, by determining the latency for the animals either to shake one of their two hind limbs or to jump. Three groups of mice were tested 60 min after intraplantar injection in each hind limb of 5 μ l of PBS, CyrTx-1a (i.e., 102 nmol·kg⁻¹) or HwTx-IV (i.e., 49 nmol·kg⁻¹), while another group of animals was tested without any injection. (a) and (b) Means \pm SD of data obtained from n mice (numbers in parentheses) under each condition. * P < 0.05, significantly different as indicated

injections, was not significantly affected, that is, 97.8 \pm 2.3% (n = 8 mice), indicating that injections of the toxin vehicle had no effect on the maximal CMAP amplitude and that no marked run-down of the response occurred.

The toxin blocking effect was quantified by establishing the concentration–response curves and determining the IC₅₀ values. As shown in Figure 8b, the concentration–response curves for CyrTx-1a and HwTx-IV revealed IC₅₀ values of 152.3 and 0.9 nmol·kg⁻¹ mouse, respectively. The five different excitability tests (stimulus–response, strength–duration, and current–threshold relationships, as well as threshold electrotonus and recovery cycle) were performed together before and 30 min after intramuscular injections of PBS solution containing CyrTx-1a (448.7 nmol·kg⁻¹ mouse), and the derived neuromuscular excitability parameters were determined (Figure S3 and Table S5). With the exception of decreased maximal CMAP amplitude and increased stimulus intensity required to generate a 50% maximal amplitude CMAP (stimulus–response relationship), analysis of strength–duration relationship, threshold electrotonus, current–threshold relationship, and recovery cycle did not reveal other CyrTx-1a effects. The CyrTx-1a-induced effects were completely reversed within 12 hr after peptide injections.

3.8 | In vivo toxicity of CyrTx-1a, compared to HwTx-IV, in mice

No deaths followed the intraplantar injection of 102 nmol kg⁻¹ of CyrTx-1a and 49 nmol kg⁻¹ of HwTx-IV in mice. In contrast, intramuscular injection of 144.4 nmol kg⁻¹ of CyrTx-1a (a concentration which produced an inhibition of ~50% of maximal CMAP amplitude), at the tail base, caused death of 50% (2/4) of animals within 1 hr. By comparison, a similar in vivo toxicity (60% of animals [3/5] died within 1 hr) was observed following injection of an approximately 3.5 times lower HwTx-IV concentration, that is, 41.4 nmol·kg⁻¹. These results strongly suggest a lower in vivo toxicity of CyrTx-1a, compared to HwTx-IV, following intramuscular injections of toxins at the base of mouse tail.

4 | DISCUSSION

This study was undertaken to identify a peptide with antinociceptive properties, among the Smartox venom collection. The strategy consisted of (a) a high throughput screening of 117 different venoms using automated patch-clamp platforms on cells overexpressing the antinociceptive target hNav1.7 and the cardiac hNav1.5 channels, (b) the isolation and identification of a new peptide, CyrTx-1a, from the *C. schioedtei* venom, (c) its structure characterization and chemical synthesis, and (d) the evaluation of the synthetic peptide functional properties using multiscale (from individual cell to in vivo) approaches.

With the identification of a large number of hits from our primary screening campaigns, a triage was performed based on potency, in both tonic- and use-dependent current inhibition protocols. The use of venoms from different species (snakes, spiders, scorpions, wasps, bees, amphibians, lizards, and fishes) provided interesting information with regard to the target on which these libraries were screened on. The most striking observation was that spider venoms contain by far the greatest number of compounds active on hNav1.7 channels with

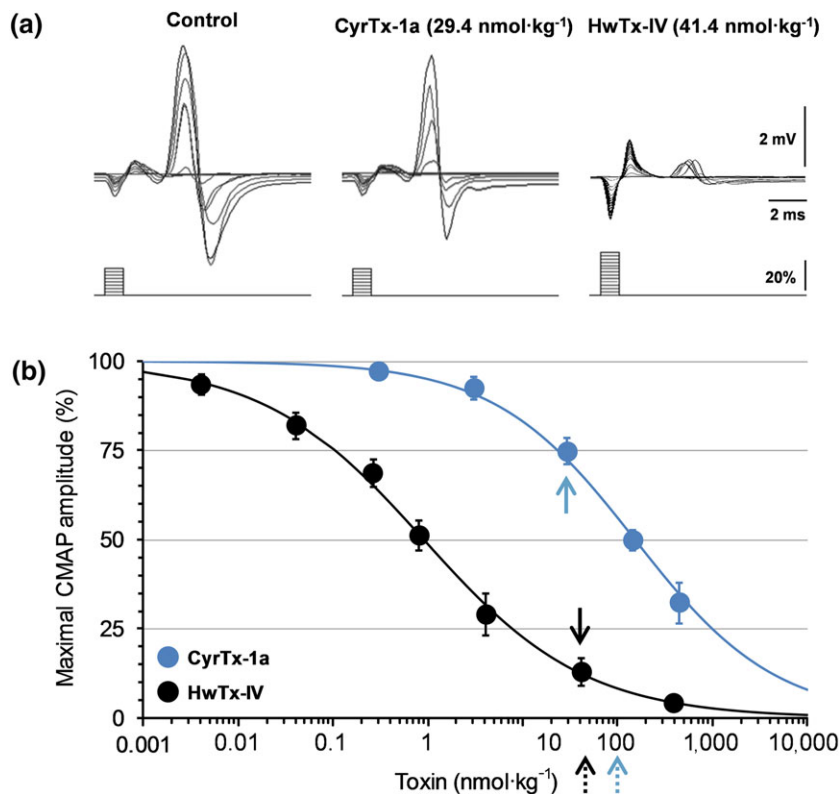


FIGURE 8 Effects of CyrTx-1a and HwTx-IV on the CMAP recorded in vivo from mouse tail muscle in response to caudal motor nerve stimulation. (a) Superimposed traces of CMAP following increasing intensities of stimulation (scheme), before (control), and after CyrTx-1a (29.4 nmol·kg⁻¹, full blue arrow in (b)) or HwTx-IV (41.4 nmol·kg⁻¹, full black arrow in (b)) injection. (b) Concentration–response curves of the effects of CyrTx-1a and HwTx-IV on the maximal CMAP amplitude. Each value, expressed as percentage of that obtained before injection, represents the mean ± SD of data obtained from four (CyrTx-1a) and five (HwTx-IV) mice. IC₅₀ and n_H values were, respectively, 152.3 nmol·kg⁻¹ and 0.6 for CyrTx-1a (r² = 0.992) and 0.9 nmol·kg⁻¹ and 0.5 for HwTx-IV (r² = 0.998). The dashed arrows indicate the toxin concentrations used for hot-plate and von Frey assays

a hit rate (for the primary screening) that was seven times higher than scorpion venoms and up to 40-fold higher than snake venoms. These data point to the impressive specialization of spider venoms for targeting Na_v channels. Based on this screening procedure, we focused our attention on CyrTx-1a which was identified in the screening and highlighted for progression in our flowchart for more extensive in vitro and in vivo investigation.

The isolation of CyrTx-1a followed a two-step purification procedure using a double in vitro-guided assay (block of hNa_v1.7 channels and inactivity on the cardiac safety-compromising hNa_v1.5 channels). Once the activity of the purified compound was confirmed by patch-clamp, the toxin entered the phase of sequence deconvolution. Any doubts on Leu or Ile residues were solved by Edman sequencing. The peptide was then synthesized and properly folded according to mass determination and coelution properties, a *sine qua non* condition for in vitro characterization and in vivo evaluation.

Despite a high sequence identity with HnTx-I (82%), CyrTx-1a shares more pharmacological properties with less similar toxins, such as HwTx-IV (42% identity) and GpTx-1 (45% identity). This is likely to be mainly due to the presence of Asn²³ instead of Ser²³ in the HnTx-I sequence that excludes any Na_v1.7 channel activity (Klint, Chin, & Mobli, 2015), while a high potency for Na_v1.7 channels associated with a good selectivity against Na_v1.5 and Na_v1.4 channels is due to the conservation of highly functional residues (Murray et al., 2015; Xiao et al., 2008). Indeed, CyrTx-1a possesses several highly conserved and crucial amino acids, known to govern the Na_v channel activity, such as the Phe⁵, Pro¹¹, Leu²⁰, Ser²³, His²⁶, and more importantly the Trp²⁸ and Lys³⁰ residues (Minassian et al., 2013; Murray

et al., 2016; Shcherbatko et al., 2016). In addition, its sequence includes a hydrophobic patch (Gly⁴, Gly⁶, and Val³¹) that has been described to reinforce the inhibitory potency of ICK toxins at Na_v1.7 channels (Agwa, Huang, Craik, Henriques, & Schroeder, 2017). Due to these similarities, CyrTx-1a may share the same binding site on TTX-sensitive Na_v channels as the one determined by mutational analysis and in silico docking for HnTx-IV, HwTx-IV, and GpTx-1a (Cai et al., 2015; Minassian et al., 2013; Murray et al., 2016). Indeed, positively charged amino acids Lys²⁵, His²⁶, Lys²⁷, and Lys³⁰, surrounded by hydrophobic Phe⁵ and Trp²⁸ clustered on one toxin face may be involved in interactions with negatively charged Glu⁷⁵³, Glu⁸¹¹, Asp⁸¹⁶, and Glu⁸¹⁸ or aliphatic residues (Met⁷⁵⁰) located in S1–S2 and S3–S4 loops of DII domain of TTX-sensitive Na_v channels (Klint et al., 2014; Li et al., 2004; Liu et al., 2012; Xiao et al., 2008; Xiao, Blumenthal, Jackson, Liang, & Cummins, 2010).

The first step to evaluate CyrTx-1a functional properties was to study the effects of the synthetic peptide on cells overexpressing hNa_v1.1–1.8 channels, using patch-clamp techniques. This study allowed (a) to test whether the potent blocking effect of the synthetic peptide, compared to the native molecule, was conserved on hNa_v1.7 channels and (b) to reinforce the evaluation of its selectivity profile on the various Na_v channels.

Synthetic (1 μM) and native (0.57 μM) CyrTx-1a produced 89.1 ± 4.1% (n = 14 wells from seven plates) and 98.8 ± 0.7% (n = 6 wells from three plates) inhibition of hNa_v1.7 channels, respectively, indicating that the two peptides were similarly, and highly, potent in interacting with this channel. The mean IC₅₀ values of CyrTx-1a interaction with hNa_v1.7 channels, obtained from automated and manual

patch-clamp experiments, were 129.5 and 52.7 nM, respectively. From this point of view and compared to toxins belonging to the NaSpTx family 1 such as HnTx-I, HnTx-III, Hd1a, HnTx-IV, ProTx-III, Cm1a, GpTx-1, and HwTx-IV previously reported to interact with this subtype, CyrTx-1a is thus among the most efficient peptides (Cardoso et al., 2015; Klint et al., 2014; Klint et al., 2015; Liu et al., 2012; Liu et al., 2013; Murray et al., 2015; Murray et al., 2016; Shcherbatko et al., 2016; Xiao et al., 2008). In addition to hNav_v1.7 channels, CyrTx-1a was also shown to be highly potent to block the TTX-S hNav_v1.1, 1.2, 1.3, and 1.6 channels with the following increasing order for mean IC₅₀ values (between approximately 75 and 300 nM): hNav_v1.1 ≈ hNav_v1.2 ≈ hNav_v1.6 ≈ hNav_v1.7 > hNav_v1.3. The recent discovery that Na_v1.1 and 1.3 channels are involved in pain pathways (Cardoso & Lewis, 2018; Chen et al., 2014; Osteen et al., 2016) and that the Na_v1.2 channel is only located in the CNS (de Lera Ruiz & Kraus, 2015) does not impair further development of CyrTx-1a as a potential antinociceptive agent to access only peripheral Na_v channel subtypes. In agreement, no central side effect was detected when the toxin was locally injected to mice for studying its action on neuromuscular system and on heat and tactile sensitivity, in vivo. In addition, the analgesic property of CyrTx-1a seems not to be associated with inhibition of hCa_v3.1 and hCa_v3.2, two channels known to be involved in pain process (Choi, Yu, Hwang, & Llinas, 2016; Sekiguchi, Tsubota, & Kawabata, 2018). Moreover, the synthetic peptide has low, at best micromolar, affinities for hNav_v1.5, hCa_v1.2, hK_v7.1, hK_v11.1, and hKir2.1 channels, well-known targets in cardiac safety (Crumb, Vicente, Johannesen, & Strauss, 2016). However, although fully sparing the skeletal muscle hNav_v1.4 channel, CyrTx-1a also targets the peripheral nerve hNav_v1.6 channel. This may represent a limitation for the in vivo efficacy of the toxin, despite the fact that this channel has been reported to be up-regulated in various peripheral pain pathways (Gonçalves, Benoit, Partiseti, & Servent, 2018). The development of analogues with improved hNav_v channel selectivity will thus be required.

The second step to evaluate CyrTx-1a functional properties was to study the peptide effects on TTX-S and TTX-R sodium currents of adult mouse DRG neurons, including mainly the TTX-S Na_v1.1, 1.6, and 1.7 channels and the TTX-R Na_v1.8 and 1.9 channels (Rush, Cummins, & Waxman, 2007). This study was motivated by the well-known physiological importance of DRG neurons in pain signalling. As expected, the preferential blocking effect of TTX-S Na_v channels by CyrTx-1a was confirmed on mouse DRG neurons since the peptide was 920 times more efficient to inhibit the peak amplitude of TTX-S than TTX-R sodium currents recorded from these neurons. These results are consistent with previous observations on adult rodent DRG neurons showing that other potential antinociceptive toxins, such as HnTx-IV, GpTx-1, and HwTx-IV, inhibit TTX-S current without markedly affecting TTX-R current (Liu et al., 2003; Murray et al., 2015; Peng, Shu, Liu, & Liang, 2002). Most of these peptides, including CyrTx-1a, inhibit hNav_v1.7 and/or TTX-S currents without any significant modification of activation and inactivation kinetics and/or voltage dependence. From a general point of view, CyrTx-1a was therefore more efficient to block TTX-S than TTX-R channels

overexpressed in HEK-293 cells, as well as TTX-S than TTX-R currents of DRG neurons. These results may suggest that the toxin interacted with the TTX receptor binding site, or the other way around, of the Na_v channel protein. However, this hypothesis is not further supported taking into account that the affinity of CyrTx-1a for the TTX-S hNav_v1.4 channel was relatively low (mean IC₅₀ of ≈8 μM).

The third step to evaluate CyrTx-1a functional properties, and to go deeper in the antinociceptive appraisal of the peptide, was to study its effects on heat and tactile sensitivity of mice in vivo, using hot-plate and von Frey assays, respectively. Following intraplantar injections, the peptide (102 nmol·kg⁻¹) was as efficient as HwTx-IV (49 nmol·kg⁻¹) in increasing the time to first pain manifestation of animals to nociceptive heat, while non-significant change was detected in the force intensity at which the mice, injected with CyrTx-1a, HwTx-IV or PBS, removed their hind limb in response to fibre pressure. Similar results were obtained from mice lacking the Na_v1.7 channels (global Na_v1.7 knockout animals) which were reported to be insensitive to thermal pain while the tactile sensitivity measured with von Frey testing was unchanged (Gingras et al., 2014). These results highlight the more pronounced involvement of the Na_v1.7 channels in heat than tactile sensitivity. The fact that CyrTx-1a also targets the Na_v1.6 channel with high affinity, a subtype located in motor axons innervating skeletal muscles (Caldwell, Schaller, Lasher, Peles, & Levinson, 2000), could limit the safe use of this peptide as an antinociceptive agent. Experiments were thus also conducted to test CyrTx-1a effects on the mouse neuromuscular system in vivo. These effects mainly consisted of CMAP inhibition, as shown in the present work and previously reported for HwTx-IV (Gonçalves, Boukaiba, et al., 2018). These results strongly suggest that the two peptides produce a marked decrease of the density of functional “transient” Na_v channels. Besides these effects, CyrTx-1a, as HwTx-IV (Gonçalves, Boukaiba, et al., 2018), did not modify other excitability parameters, indicating that the peptide does not affect the density of other functional ion channels, receptors, and pumps, nor the passive membrane properties of the neuromuscular system (Kiernan & Bostock, 2000; Krishnan et al., 2008). CyrTx-1a was approximately 170 times less efficient than HwTx-IV to inhibit CMAP. Assuming that both toxins have also similar affinity on the mouse Na_v1.6 channels, we infer that the accessibility to this subtype, located mainly at the nodes of Ranvier of motor myelinated axons (Caldwell et al., 2000), is somehow more limited for CyrTx-1a than for HwTx-IV.

In conclusion, the present results highlight that CyrTx-1a purified from *C. schioedtei* spider venom is a new toxin interacting with hNav_v1.7 channels associated with an antinociceptive effect. Further structure–activity relationships and engineering studies will be necessary to improve the Na_v channel selectivity profile and analgesic potency of CyrTx-1a. In particular, it is likely that synthetic modified homologues, associated with molecular dynamics simulation using CyrTx-1a and Na_v channels, will reinforce the potential use of the peptide as a lead molecule for the potential development of novel pain therapeutic agents.

ACKNOWLEDGEMENTS

This research was funded by a collaborative grant (#153114) between Sanofi Research & Development (Chilly-Mazarin, France) and the French Alternative Energies and Atomic Energy Commission (CEA, Gif-sur-Yvette, France). M.D.W. acknowledges financial support from the French Agence Nationale de la Recherche (Grant ANR-11-LABX-0015). T.C.G. was supported by a doctoral CIFRE fellowship from Sanofi. The authors wish to thank Dr. Muriel AMAR (CEA de Saclay, Gif-sur-Yvette, France) for her help in the calculation of kinetic parameters of sodium current activation and inactivation and Dr. Isabel LEFEVRE (Sanofi R&D, Chilly-Mazarin, France) for her critical reading of the manuscript.

AUTHOR CONTRIBUTIONS

L.L. performed experiments and J.M.C. analysed the data for the venom fraction screenings. S.C. and L.J. performed experiments and M.D.W. and R.Bé. analysed the data for the peptide purification, sequencing, and synthesis experiments. T.C.G., S.F., R.Bo., B.S., A.B., and M.P. performed and analysed experiments done on recombinant ion channel cell lines. T.C.G. and E.B. performed and analysed experiments done on DRG neurons and mice. M.K. and G.H. determined 3D structure. L.B. and S.H. aided in the preparation of the manuscript. T.C.G., E.B., M.P., M.D.W., and D.S. wrote the manuscript and supervised the study. All authors approved the manuscript.

CONFLICT OF INTEREST

The authors L.B., A.B., R.B., J.M.C., S.F., T.C.G., G.H., S.H., M.K., L.L., B.S., and M.P. declare the following competing interest: current or former employees of Sanofi.

DECLARATION OF TRANSPARENCY AND SCIENTIFIC RIGOUR

This Declaration acknowledges that this paper adheres to the principles for transparent reporting and scientific rigour of preclinical research as stated in the BJP guidelines for [Design & Analysis](#), and [Animal Experimentation](#), and as recommended by funding agencies, publishers and other organisations engaged with supporting research.

ORCID

Evelyne Benoit  <https://orcid.org/0000-0001-5501-0888>

Denis Servent  <https://orcid.org/0000-0002-0774-1691>

REFERENCES

- Agwa, A. J., Huang, Y. H., Craik, D. J., Henriques, S. T., & Schroeder, C. I. (2017). Lengths of the C-terminus and interconnecting loops impact stability of spider-derived gating modifier toxins. *Toxins*, *9*, 248–263.
- Alexander, S. P., Striessnig, J., Kelly, E., Marrion, N. V., Peters, J. A., Faccenda, E., ... CGTP Collaborators (2017). The concise guide to pharmacology 2017/18: Voltage-gated ion channels. *British Journal of Pharmacology*, *174*, S160–S194. <https://doi.org/10.1111/bph.13884>
- Bennett, D. L., & Woods, C. G. (2014). Painful and painless channelopathies. *Lancet Neurology*, *13*, 587–599. [https://doi.org/10.1016/S1474-4422\(14\)70024-9](https://doi.org/10.1016/S1474-4422(14)70024-9)
- Cai, T., Luo, J., Meng, E., Ding, J., Liang, S., Wang, S., & Liu, Z. (2015). Mapping the interaction site for the tarantula toxin hainantoxin-IV (β -TRTX-Hn2a) in the voltage sensor module of domain II of voltage-gated sodium channels. *Peptides*, *68*, 148–156. <https://doi.org/10.1016/j.peptides.2014.09.005>
- Caldwell, J. H., Schaller, K. L., Lasher, R. S., Peles, E., & Levinson, S. R. (2000). Sodium channel Na(v)1.6 is localized at nodes of ranvier, dendrites, and synapses. *Proceedings of the National Academy of Sciences of the United States of America*, *97*, 5616–5620. <https://doi.org/10.1073/pnas.090034797>
- Capasso, A., Di Giannuario, A., Loizzo, A., Pieretti, S., & Sorrentino, L. (1994). Dexamethasone influence on morphine-induced analgesia in outbred Swiss and inbred DBA/2J and C57BL/6 mice. *Progress in Neuro-Psychopharmacology & Biological Psychiatry*, *18*, 779–792. [https://doi.org/10.1016/0278-5846\(94\)90084-1](https://doi.org/10.1016/0278-5846(94)90084-1)
- Cardoso, F. C., Dekan, Z., Rosengren, K. J., Erickson, A., Vetter, I., Deuis, J. R., ... Lewis, R. J. (2015). Identification and characterization of ProTx-III [mu-TRTX-Tp1a], a new voltage-gated sodium channel inhibitor from venom of the tarantula *Thrixopelma pruriens*. *Molecular Pharmacology*, *88*, 291–303. <https://doi.org/10.1124/mol.115.098178>
- Cardoso, F. C., Dekan, Z., Smith, J. J., Deuis, J. R., Vetter, I., Herzig, V., ... Lewis, R. J. (2017). Modulatory features of the novel spider toxin mu-TRTX-Df1a isolated from the venom of the spider *Davus fasciatus*. *British Journal of Pharmacology*, *174*, 2528–2544. <https://doi.org/10.1111/bph.13865>
- Cardoso, F. C., & Lewis, R. J. (2018). Sodium channels and pain: From toxins to therapies. *British Journal of Pharmacology*, *175*, 2138–2157. <https://doi.org/10.1111/bph.13962>
- Catterall, W. A., Goldin, A. L., & Waxman, S. G. (2005). International Union of Pharmacology. XLVII. Nomenclature and structure-function relationships of voltage-gated sodium channels. *Pharmacological Reviews*, *57*, 397–409. <https://doi.org/10.1124/pr.57.4.4>
- Cerles, O., Benoit, E., Chereau, C., Chouzenoux, S., Morin, F., Guillaumot, M. A., ... Nicco, C. (2017). Niclosamide inhibits oxaliplatin neurotoxicity while improving colorectal cancer therapeutic response. *Molecular Cancer Therapeutics*, *16*, 300–311. <https://doi.org/10.1158/1535-7163.MCT-16-0326>
- Chen, H. P., Zhou, W., Kang, L. M., Yan, H., Zhang, L., Xu, B. H., & Cai, W. H. (2014). Intrathecal miR-96 inhibits Na_v1.3 expression and alleviates neuropathic pain in rat following chronic constriction injury. *Neurochemical Research*, *39*, 76–83. <https://doi.org/10.1007/s11064-013-1192-z>
- Choi, S., Yu, E., Hwang, E., & Llinas, R. R. (2016). Pathophysiological implication of CaV3.1 T-type Ca²⁺ channels in trigeminal neuropathic pain. *Proceedings of the National Academy of Sciences of the United States of America*, *113*, 2270–2275. <https://doi.org/10.1073/pnas.1600418113>
- Crumb, W. J. Jr., Vicente, J., Johannesen, L., & Strauss, D. G. (2016). An evaluation of 30 clinical drugs against the comprehensive in vitro proarrhythmia assay (CiPA) proposed ion channel panel. *Journal Of Pharmacological And Toxicological Methods*, *81*, 251–262. <https://doi.org/10.1016/j.vascn.2016.03.009>
- Deuis, J. R., Wingerd, J. S., Winter, Z., Durek, T., Dekan, Z., Sousa, S. R., ... Vetter, I. (2016). Analgesic effects of GpTx-1, PF-04856264 and CNV1014802 in a mouse model of Na_v1.7-mediated pain. *Toxins*, *8*, 78–87. <https://doi.org/10.3390/toxins8030078>
- Dib-Hajj, S. D., Yang, Y., Black, J. A., & Waxman, S. G. (2013). The Na_v1.7 sodium channel: From molecule to man. *Nature Reviews. Neuroscience*, *14*, 49–62. <https://doi.org/10.1038/nrn3404>
- Flinspach, M., Xu, Q., Piekarz, A. D., Fellows, R., Hagan, R., Gibbs, A., ... Wickenden, A. D. (2017). Insensitivity to pain induced by a potent

- selective closed-state $\text{Na}_v1.7$ inhibitor. *Scientific Reports*, 7, 39662. <https://doi.org/10.1038/srep39662>
- Gingras, J., Smith, S., Matson, D. J., Johnson, D., Nye, K., Couture, L., ... McDonough, S. I. (2014). Global $\text{Na}_v1.7$ knockout mice recapitulate the phenotype of human congenital indifference to pain. *PLoS ONE*, 9, e105895. <https://doi.org/10.1371/journal.pone.0105895>
- Gonçalves, T. C., Benoit, E., Partiseti, M., & Servent, D. (2018). The $\text{Na}_v1.7$ channel subtype as an antinociceptive target for spider toxins in adult dorsal root ganglia neurons. *Frontiers in Pharmacology*, 9, 1000. <https://doi.org/10.3389/fphar.2018.01000>
- Gonçalves, T. C., Boukaiba, R., Molgo, J., Amar, M., Partiseti, M., Servent, D., & Benoit, E. (2018). Direct evidence for high affinity blockade of $\text{Na}_v1.6$ channel subtype by huwentoxin-IV spider peptide, using multiscale functional approaches. *Neuropharmacology*, 133, 404–414. <https://doi.org/10.1016/j.neuropharm.2018.02.016>
- Hagen, N. A., Cantin, L., Constant, J., Haller, T., Blaise, G., Ong-Lam, M., ... Lapointe, B. (2017). Tetrodotoxin for moderate to severe cancer-related pain: A multicentre, randomized, double-blind, placebo-controlled, parallel-design trial. *Pain Research & Management*, 2017(7212713), 1–7. <https://doi.org/10.1155/2017/7212713>
- Harding, S. D., Sharman, J. L., Faccenda, E., Southan, C., Pawson, A. J., Ireland, S., ... NC-IUPHAR (2018). The IUPHAR/BPS Guide to pharmacology in 2018: Updates and expansion to encompass the new guide to immunopharmacology. *Nucleic Acids Research*, 46, D1091–D1106. <https://doi.org/10.1093/nar/gkx1121>
- Israel, M. R., Tay, B., Deus, J. R., & Vetter, I. (2017). Sodium channels and venom peptide pharmacology. *Advances in Pharmacology*, 79, 67–116. <https://doi.org/10.1016/bs.apha.2017.01.004>
- Kiernan, M. C., & Bostock, H. (2000). Effects of membrane polarization and ischaemia on the excitability properties of human motor axons. *Brain*, 123, 2542–2551. <https://doi.org/10.1093/brain/123.12.2542>
- Kilkenny, C., Browne, W., Cuthill, I. C., Emerson, M., & Altman, D. G. (2010). Animal research: Reporting in vivo experiments: The ARRIVE guidelines. *British Journal of Pharmacology*, 160, 1577–1579.
- Klint, J. K., Berecki, G., Durek, T., Mobli, M., Knapp, O., King, G. F., ... Rash, L. D. (2014). Isolation, synthesis and characterization of omega-TRTX-Cc1a, a novel tarantula venom peptide that selectively targets L-type Cav channels. *Biochemical Pharmacology*, 89, 276–286. <https://doi.org/10.1016/j.bcp.2014.02.008>
- Klint, J. K., Chin, Y. K. Y., & Mobli, M. (2015). Rational engineering defines a molecular switch that is essential for activity of spider-venom peptides against the analgesics target $\text{Na}_v1.7$. *Molecular Pharmacology*, 88, 1002–1010. <https://doi.org/10.1124/mol.115.100784>
- Klint, J. K., Senff, S., Rupasinghe, D. B., Er, S. Y., Herzig, V., Nicholson, G. M., & King, G. F. (2012). Spider-venom peptides that target voltage-gated sodium channels: pharmacological tools and potential therapeutic leads. *Toxicon*, 60, 478–491.
- Krishnan, A. V., Lin, C. S. Y., Park, S. B., & Kiernan, M. C. (2008). Assessment of nerve excitability in toxic and metabolic neuropathies. *Journal of the Peripheral Nervous System*, 13, 7–26. <https://doi.org/10.1111/j.1529-8027.2008.00155.x>
- de Lera Ruiz, M., & Kraus, R. L. (2015). Voltage-gated sodium channels: Structure, function, pharmacology, and clinical indications. *Journal of Medicinal Chemistry*, 58, 7093–7118. <https://doi.org/10.1021/jm501981g>
- Li, D., Xiao, Y., Xu, X., Xiong, X., Lu, S., Liu, Z., ... Liang, S. (2004). Structure-activity relationships of hainantoxin-IV and structure determination of active and inactive sodium channel blockers. *The Journal of Biological Chemistry*, 279, 37734–37740. <https://doi.org/10.1074/jbc.M405765200>
- Liu, Y., Li, D., Wu, Z., Li, J., Nie, D., Xiang, Y., & Liu, Z. (2012). A positively charged surface patch is important for hainantoxin-IV binding to voltage-gated sodium channels. *Journal of Peptide Science*, 18, 643–649. <https://doi.org/10.1002/psc.2451>
- Liu, Z., Cai, T., Zhu, Q., Deng, M., Li, J., Zhou, X., ... Liang, S. (2013). Structure and function of hainantoxin-III, a selective antagonist of neuronal tetrodotoxin-sensitive voltage-gated sodium channels isolated from the Chinese bird spider *Ornithoctonus hainana*. *The Journal of Biological Chemistry*, 288, 20392–20403. <https://doi.org/10.1074/jbc.M112.426627>
- Liu, Z., Dai, J., Chen, Z., Hu, W., Xiao, Y., & Liang, S. (2003). Isolation and characterization of hainantoxin-IV, a novel antagonist of tetrodotoxin-sensitive sodium channels from the Chinese bird spider *Selenocosmia hainana*. *Cellular and Molecular Life Sciences*, 60, 972–978. <https://doi.org/10.1007/s00018-003-2354-x>
- Minassian, N. A., Gibbs, A., Shih, A. Y., Liu, Y., Neff, R. A., Sutton, S. W., ... Wickenden, A. D. (2013). Analysis of the structural and molecular basis of voltage-sensitive sodium channel inhibition by the spider toxin huwentoxin-IV (mu-TRTX-Hh2a). *The Journal of Biological Chemistry*, 288, 22707–22720. <https://doi.org/10.1074/jbc.M113.461392>
- Mogil, J. S. (2012). Sex differences in pain and pain inhibition: Multiple explanations of a controversial phenomenon. *Nature Reviews. Neuroscience*, 13, 859–866. <https://doi.org/10.1038/nrn3360>
- Moyer, B. D., Murray, J. K., Ligutti, J., Andrews, K., Favreau, P., Jordan, J. B., ... Miranda, L. P. (2018). Pharmacological characterization of potent and selective $\text{Na}_v1.7$ inhibitors engineered from *Chilobrachys jingzhao* tarantula venom peptide JzTx-V. *PLoS ONE*, 13, e0196791. <https://doi.org/10.1371/journal.pone.0196791>
- Murray, J. K., Ligutti, J., Liu, D., Zou, A., Poppe, L., Li, H., ... Miranda, L. P. (2015). Engineering potent and selective analogues of GpTx-1, a tarantula venom peptide antagonist of the $\text{Na}_v1.7$ sodium channel. *Journal of Medicinal Chemistry*, 58, 2299–2314. <https://doi.org/10.1021/jm501765v>
- Murray, J. K., Long, J., Zou, A., Ligutti, J., Andrews, K. L., Poppe, L., ... Miranda, L. P. (2016). Single residue substitutions that confer voltage-gated sodium ion channel subtype selectivity in the $\text{Na}_v1.7$ inhibitory peptide GpTx-1. *Journal of Medicinal Chemistry*, 59, 2704–2717. <https://doi.org/10.1021/acs.jmedchem.5b01947>
- Osteen, J. D., Herzig, V., Gilchrist, J., Emrick, J. J., Zhang, C., Wang, X., ... Julius, D. (2016). Selective spider toxins reveal a role for the $\text{Na}_v1.1$ channel in mechanical pain. *Nature*, 534, 494–499. <https://doi.org/10.1038/nature17976>
- Peng, K., Shu, Q., Liu, Z., & Liang, S. (2002). Function and solution structure of huwentoxin-IV, a potent neuronal tetrodotoxin (TTX)-sensitive sodium channel antagonist from Chinese bird spider *Selenocosmia huwena*. *The Journal of Biological Chemistry*, 277, 47564–47571. <https://doi.org/10.1074/jbc.M204063200>
- Rush, A. M., Cummins, T. R., & Waxman, S. G. (2007). Multiple sodium channels and their roles in electrogenesis within dorsal root ganglion neurons. *The Journal of Physiology*, 579, 1–14. <https://doi.org/10.1113/jphysiol.2006.121483>
- Saez, N. J., Senff, S., Jensen, J. E., Er, S. Y., Herzig, V., Rash, L. D., & King, G. F. (2010). Spider-venom peptides as therapeutics. *Toxins*, 2, 2851–2871. <https://doi.org/10.3390/toxins2122851>
- Sekiguchi, F., Tsubota, M., & Kawabata, A. (2018). Involvement of voltage-gated calcium channels in inflammation and inflammatory pain. *Biological & Pharmaceutical Bulletin*, 41, 1127–1134. <https://doi.org/10.1248/bpb.b18-00054>
- Shcherbatko, A., Rossi, A., Foletti, D., Zhu, G., Bogin, O., Galindo Casas, M., ... Strop, P. (2016). Engineering highly potent and selective microproteins against $\text{Na}_v1.7$ sodium channel for treatment of pain.

The Journal of Biological Chemistry, 291, 13974–13986. <https://doi.org/10.1074/jbc.M116.725978>

Vetter, I., Deuis, J. R., Mueller, A., Israel, M. R., Starobova, H., Zhang, A., ... Mobli, M. (2017). Na_v1.7 as a pain target—From gene to pharmacology. *Pharmacology & Therapeutics*, 172, 73–100. <https://doi.org/10.1016/j.pharmthera.2016.11.015>

Waxman, S. G., & Zamponi, G. W. (2014). Regulating excitability of peripheral afferents: Emerging ion channel targets. *Nature Neuroscience*, 17, 153–163. <https://doi.org/10.1038/nn.3602>

Xiao, Y., Bingham, J. P., Zhu, W., Moczydlowski, E., Liang, S., & Cummins, T. R. (2008). Tarantula huwentoxin-IV inhibits neuronal sodium channels by binding to receptor site 4 and trapping the domain II voltage sensor in the closed configuration. *The Journal of Biological Chemistry*, 283, 27300–27313. <https://doi.org/10.1074/jbc.M708447200>

Xiao, Y., Blumenthal, K., Jackson, J. O. 2nd, Liang, S., & Cummins, T. R. (2010). The tarantula toxins ProTx-II and huwentoxin-IV differentially interact with human Na_v1.7 voltage sensors to inhibit channel

activation and inactivation. *Molecular Pharmacology*, 78, 1124–1134. <https://doi.org/10.1124/mol.110.066332>

SUPPORTING INFORMATION

Additional supporting information may be found online in the Supporting Information section at the end of the article.

How to cite this article: Gonçalves TC, Benoit E, Kurz M, et al. From identification to functional characterization of cyriotoxin-1a, an antinociceptive toxin from the spider *Cyriopagopus schioedtei*. *Br J Pharmacol*. 2019;176:1298–1314. <https://doi.org/10.1111/bph.14628>

Supporting information for:

From identification to functional characterization of cyriotoxin-1a, an antinociceptive toxin from *Cyriopagopus schioedtei* spider

Tânia C. Gonçalves^{†,‡}, Evelyne Benoit^{‡,‡}, Michael Kurz[‡], Laetitia Lucarain[‡], Sophie Fontaine[‡], Stéphanie Combemale[‡], Lucie Jaquillard[‡], Brigitte Schombert[‡], Jean-Marie Chambard[‡], Rachid Boukaiba[‡], Gerhard Hessler[‡], Andrees Bohme[‡], Laurent Bialy[‡], Stéphane Hourcade[‡], Rémy Bérourd[‡], Michel De Waard^{‡,§}, Denis Servent^{‡,*}, Michel Partiseti^{‡,*}

[†] Sanofi R & D, Integrated Drug Discovery – High Content Biology, F-94440 Vitry-sur-Seine, France.

[#] Service d'Ingénierie Moléculaire des Protéines (SIMOPRO), CEA, Université Paris-Saclay, F-91191 Gif sur Yvette, France.

[‡] Institut des Neurosciences Paris-Saclay (Neuro-PSI), UMR CNRS/Université Paris-Sud 9197, Université Paris-Saclay, F-91198 Gif sur Yvette, France.

[‡] Sanofi R & D, Integrated Drug Discovery – Synthetic Molecular Design, Frankfurt, Germany.

[‡] Smartox Biotechnology, 6 rue des Platanes, 38120 Saint-Egrève, France.

[‡] Sanofi R & D, Neuroscience Therapeutic Area, Neurodegeneration Research, F-91385 Chilly-Mazarin, France.

[§] Institut du Thorax, Inserm UMR 1087 / CNRS UMR 6291, LabEx “Ion Channels, Science & Therapeutics”, F-44007 Nantes, France.

Table S1. Fragments sequenced by LC-MS/MS analyses of the CyrTx-1a digests. Symbol * indicates C-terminal amidation, and all cysteine residues were detected as carbamidomethyl derivatives with the addition of 57 Da.

	Sequence	Mass	<i>m/z</i>	Relative error
Trypsin digestion	SCVPGK	646.3109	324.1636	2.9 ppm
	HKWCK	757.3694	379.6914	-1.6 ppm
	ECKGFGK	824.3851	413.1994	-1.0 ppm
	SGLTCSNK	865.3964	433.7061	1.5 ppm
	CSGLTCSNK	1025.4270	513.7209	0.3 ppm
	SCVPGKNEC	1049.4270	525.7209	0.3 ppm
	SCVPGKNECC	1209.4576	605.7358	-0.4 ppm
	NECCSGLTCSNK	1428.5432	715.2799	1.4 ppm
	PGK NECCSGLTCSNK	1710.7124	856.3679	5.1 ppm
	SCVPGKNECCSGLTCSNK	2056.8435	1029.4368	7.5 ppm
	SCVPGKNECCSGLTCSNKHK	2321.9973	775.0079	2.0 ppm
Glu-C	ECKGFGKSCVPGKNE	1695.7709	566.2644	0.3 ppm
	CCSGLTCSNKHKWCKVLL*	2249.0691	1125.5420	0.2 ppm

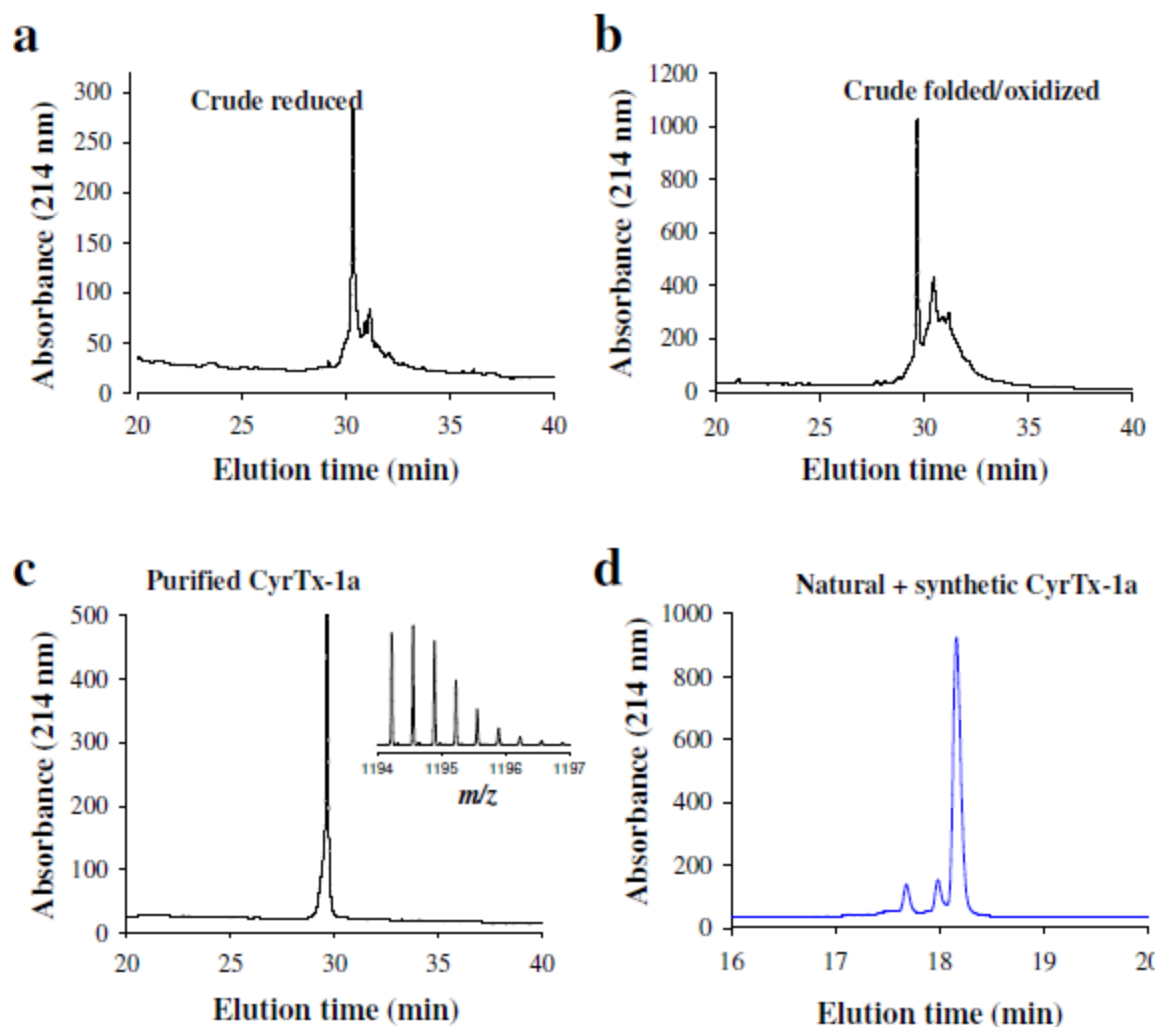


Figure S1. Chemical synthesis and refolding of CyrTx-1a. **(a)** Crude CyrTx-1a synthesis as revealed by a C18 reversed-phase chromatography. **(b)** Crude folded/oxidized CyrTx-1a. **(c)** Purified folded/oxidized CyrTx-1a illustrating the purity of the synthetic compound. Inset: illustrates the MS of synthetic CyrTx-1a of m/z 1193.8556 $[M+3H]^{3+}$. **(d)** C18 coelution profile of natural CyrTx-1a (4 μ g) mixed with synthetic CyrTx-1a (4 μ g). The presence of a single uniform peak demonstrates the identity of both compounds. The two contaminating peaks preceding the major peak represent contaminants from the natural peptide.

Table S2. ¹H-chemical shifts of CyrTx-1a in H₂O/D₂O, 50 mM phosphate buffer, pH 5.0 at 305°K (concentration: 6 mg/mL)*.

No.	Residue	NH	H α	H β	Others
1	Glu	-	4.17	2.17	γ : 2.53
2	Cys	8.74	4.89	3.26/2.95	
3	Lys	8.86	4.39	1.82/1.71	γ : 1.60/1.41, δ : 1.78/ 1.50, ϵ : 2.99
4	Gly	8.05	4.08/3.68		
5	Phe	8.45	3.79	3.07/2.82	δ : 7.10, ϵ : 7.44, ζ : 7.34
6	Gly	8.78	3.55/2.73		
7	Lys	7.66	4.44	2.05/1.83	γ : 1.48/1.19, δ : 1.62, ϵ : 3.02/2.96
8	Ser	8.48	4.93	4.01/3.96	
9	Cys	8.17	4.97	3.17/2.95	
10	Val	8.42	4.38	1.79	γ : 0.96, γ' : 0.90
11	Pro	-	4.01	2.30/1.93	γ : 2.16/1.74, δ : 4.07/3.77
12	Gly	9.19	4.33/3.78		
13	Lys	7.54	4.50	2.03/1.80	γ : 1.42/1.28, δ : 1.60, ϵ : 2.98/2.94
14	Asn	8.81	4.72	3.08/2.72	NH ₂ : 7.60/6.89
15	Glu	9.03	4.28	2.11/2.02	γ : 2.27
16	Cys	8.55	5.18	3.06/2.87	
17	Cys	9.14	4.54	3.46/2.59	
18	Ser	8.26	4.255	3.89/3.86	
19	Gly	8.95	4.40/3.72		
20	Leu	8.19	5.38	2.30/1.31	γ : 1.47, δ : 0.91, δ' : 0.87
21	Thr	9.29	4.62	3.98	γ : 1.02
22	Cys	8.83	4.68	3.19/2.98	
23	Ser	8.35	4.49	4.05/3.75	
24	Asn	9.09	4.27	2.79/2.70	NH ₂ : 7.62/6.98
25	Lys	7.89	4.01	1.51/1.21	γ : 1.07/0.84, δ : 1.51, ϵ : 2.86
26	His	7.68	4.26	1.52/1.41	δ : 7.16, ϵ : 8.60
27	Lys	8.19	3.99	2.34/2.02	γ : 1.22, δ : 1.70/1.60, ϵ : 2.97
28	Trp	6.93	5.59	3.10/2.53	H1: 10.26, H2: 6.89, H4: 7.35, H5: 7.02, H6: 7.01, H7: 7.01
29	Cys	8.58	5.00	3.28/2.69	
30	Lys	9.67	5.02	2.14/1.83	γ : 1.55/1.31, δ : 1.78/1.71, ϵ : 2.92
31	Val	8.45	4.10	2.09	γ : 1.05, γ' : 1.00
32	Leu	8.17	4.32	1.60/1.21	γ : 1.43, δ : 0.91, δ' : 0.88
33	Leu	8.28	4.39	1.68/1.58	γ : 1.64, δ : 0.95, δ' : 0.89, NH ₂ : 7.56/7.03

*: Proton chemical shifts are referenced to sodium-3-(Trimethylsilyl)propionate-2,2,3,3-d₄.

Table S3. Parameters of steady-state inactivation- ($V_{P50\%}$ and k_h) and conductance- ($V_{T50\%}$ and k_g) voltage relationships for HEK-293 cells overexpressing the hNav1.7 channel subtype (means \pm S.D. of 5 cells) and mouse DRG neurons displaying endogenous TTX-S sodium current (means \pm S.D. of 8 neurons).

	$V_{P50\%}$ (mV)	k_h (mV^{-1})	$V_{T50\%}$ (mV)	k_g (mV^{-1})
hNav1.7 current before CyrTx-1a perfusion	-73 ± 2	5.4 ± 0.3	-25 ± 4	4.5 ± 0.8
hNav1.7 current after CyrTx-1a perfusion ¹	-74 ± 3	5.6 ± 0.4	-26 ± 2	4.2 ± 0.9
TTX-S current before CyrTx-1a perfusion	-84 ± 2	8.8 ± 0.4	-37 ± 2	3.9 ± 0.2
TTX-S current after CyrTx-1a perfusion ²	-85 ± 1	9.1 ± 0.3	-33 ± 1	5.2 ± 0.3

¹ 50 nM and ² 0.25-0.5 μ M.

Table S4. Kinetic parameters of activation (t_p) and inactivation (τ_h) of endogenous TTX-S sodium current recorded from DRG neurons under the indicated conditions (means \pm S.D. of 8 cells).

	t_p (ms)	τ_h (ms)
TTX-S current after TTX ¹ wash-out	1.36 ± 0.22	0.86 ± 0.20
TTX-S current after CyrTx-1a perfusion ²	1.41 ± 0.30 ³	1.01 ± 0.31 ³

¹ 100 nM, ² 0.25-0.5 μ M. ³ $P < 0.05$ (*versus* current after TTX wash-out).

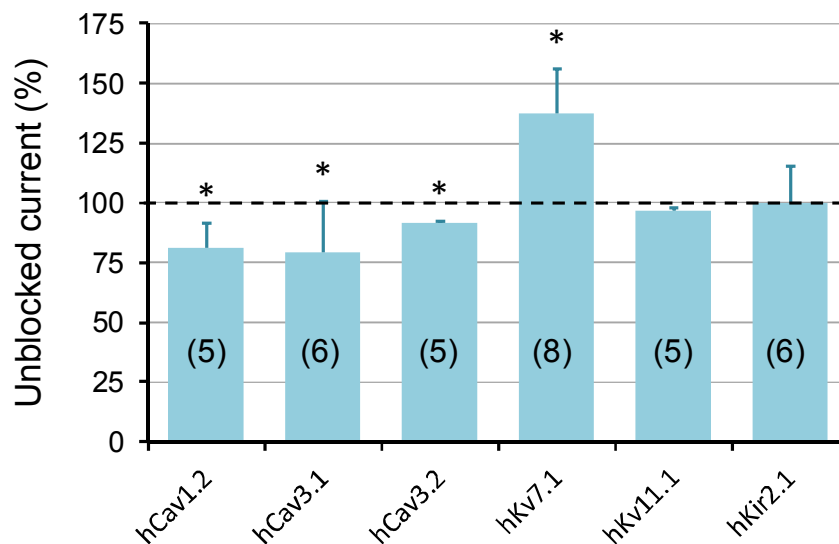


Figure S2. Effects of CyrTx-1a on HEK-293, CHO and U2OS cells overexpressing hCav1.2, 3.1 and 3.2, hKv7.1 and 11.1 and hKir2.1 channel subtypes, using whole-cell automated patch-clamp. Histograms of unblocked current, expressed as percentage of control. Each value represents the mean \pm S.D. of data obtained from n cells (numbers in parentheses). *: $P < 0.05$ *versus* control.

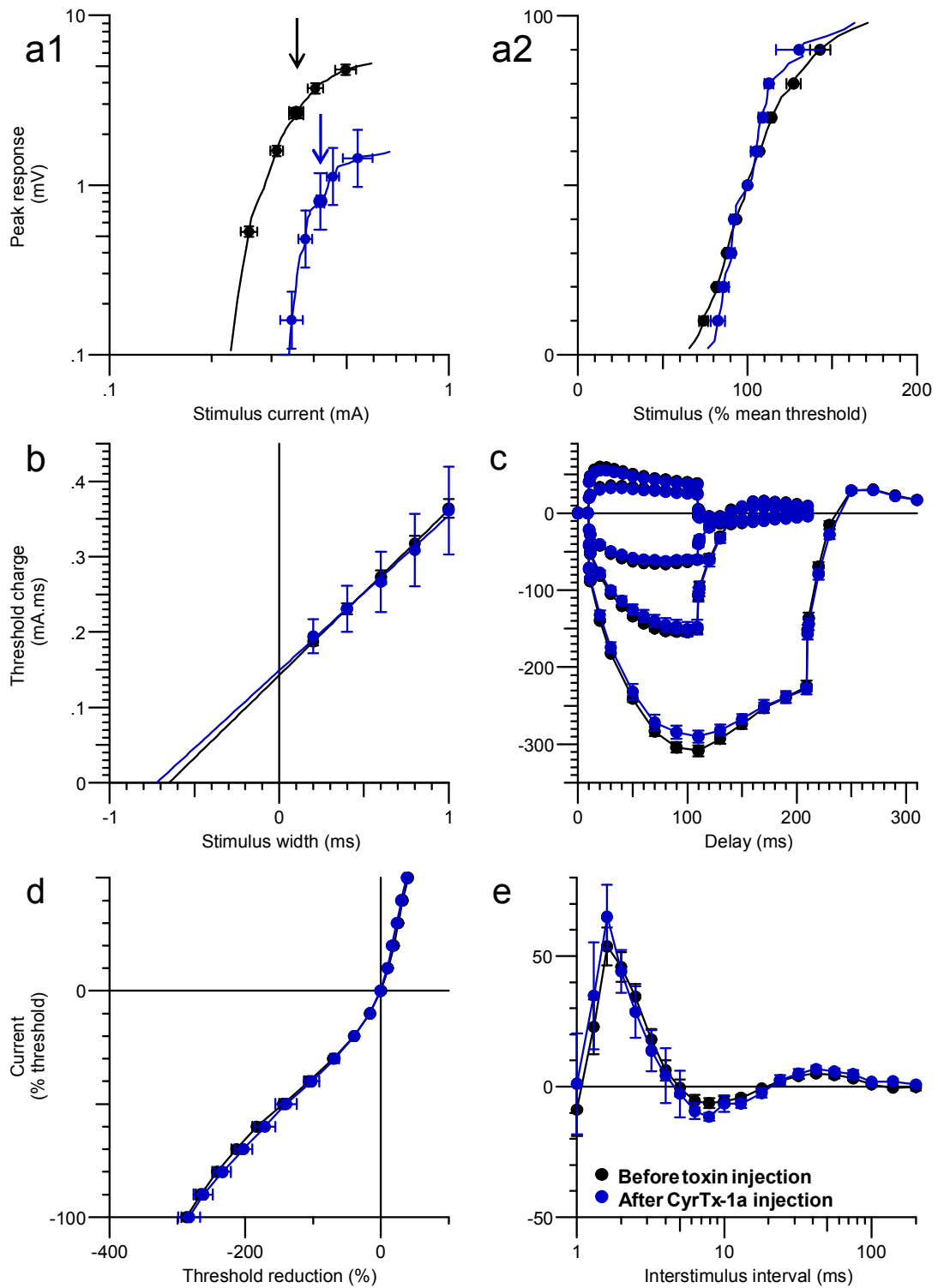


Figure S3. Superimposed excitability curves obtained *in vivo* by stimulating the mouse caudal motor nerve and recording the CMAP from tail muscle before (black circles, $n = 29$ mice) and ~ 30 min after injections of CyrTx-1a (448.7 nmol/kg mouse, blue circles, $n = 4$ mice). Data are represented as means \pm S.D. (a) stimulus-response relationships [absolute (a1) and relative (a2) CMAP amplitudes], (b) strength-duration relationship, (c) threshold electrotonus, (d) current-threshold relationship, and (e) recovery cycle. In a1, arrows indicate stimulus currents for 50% maximal response.

Table S5. Comparison of neuromuscular excitability parameters (means \pm S.D.) from mouse tail muscle recordings before toxin injections (control, n = 29 mice) and ~30 min after injections of CyrTx-1a (448.7 nmol/kg mouse, n = 4 mice).

	Excitability parameter ²	Before toxin Injection	After CyrTx-1a injection
a¹	Peak response (mV)	5.31 \pm 0.57	1.60 \pm 0.47
a	Latency (ms)	3.89 \pm 0.06	4.05 \pm 0.15
a	Stimulus (mA) for 50% max response	0.35 \pm 0.05	0.42 \pm 0.03
a	Stimulus-response slope	3.11 \pm 0.18	3.42 \pm 0.15
b¹	Strength-duration time constant (ms)	0.69 \pm 0.12	0.88 \pm 0.12
b	Rheobase (mA)	0.21 \pm 0.04	0.18 \pm 0.09
c¹	TEd (10-20 ms, 40%)	59.53 \pm 1.27	54.93 \pm 2.57
c	TEd (peak, 40%)	59.00 \pm 1.17	54.95 \pm 2.33
c	TEd (peak, 20%)	35.81 \pm 0.75	32.99 \pm 1.61
c	TEd (40-60 ms, 40%)	47.92 \pm 1.14	45.25 \pm 2.01
c	TEd (90-100 ms, 40%)	39.52 \pm 1.27	37.49 \pm 1.55
c	Accommodation half-time (ms, 40%)	46.02 \pm 0.93	45.66 \pm 2.28
c	TEd (undershoot, 40%)	-15.34 \pm 1.01	-13.64 \pm 1.57
c	TEh (10-20 ms, -40%)	-93.31 \pm 1.12	-88.95 \pm 4.09
c	TEh (20-40 ms, -40%)	-120.1 \pm 1.9	-113.3 \pm 5.7
c	TEh (90-100 ms, -40%)	-152.7 \pm 5.2	-149.3 \pm 9.2
c	TEh (slope 101-140 ms, -40%)	2.62 \pm 0.17	2.75 \pm 0.25
c	TEh (peak, -70%)	-312.4 \pm 6.7	-291.3 \pm 16.2
c	TEh (overshoot, -40%)	17.33 \pm 1.05	15.89 \pm 1.77
d¹	Resting slope	0.89 \pm 0.09	0.88 \pm 0.12
d	Minimum slope	0.23 \pm 0.01	0.23 \pm 0.02
d	Hyperpolarization slope	0.49 \pm 0.03	0.44 \pm 0.06
e¹	Refractoriness at 2 ms (%)	45.82 \pm 5.60	44.08 \pm 8.16
e	Refractoriness at 2.5 ms (%)	34.48 \pm 4.78	28.58 \pm 9.97
e	Relative refractory period (ms)	4.38 \pm 1.09	4.09 \pm 1.17
e	Superexcitability (%)	-19.00 \pm 3.91	-13.93 \pm 4.05
e	Superexcitability at 5 ms (%)	-0.49 \pm 3.26	-2.75 \pm 8.92
e	Superexcitability at 7 ms (%)	-5.94 \pm 2.06	-10.46 \pm 2.16
e	Subexcitability (%)	5.60 \pm 1.09	6.43 \pm 1.15

¹ a: stimulus-response relationship, b: strength-duration relationship, c: threshold electrotonus, d: current-threshold relationship, and e: recovery cycle. ² TEd: threshold electrotonus from depolarizing currents and TEh: threshold electrotonus from hyperpolarizing currents. Differences *versus* control are highlighted in blue.

SUPPLEMENTARY EXPERIMENTAL SECTION

Protocols for amino acid sequencing of CyrTx-1a. A Waters Q-TOF Xevo G2S mass spectrometer equipped with an Acquity UHPLC system and Lockspray source was used for the acquisition of the LC-ESI-MS and LC-ESI-MS/MS data. Five μL of each digested peptide sample was injected into an Acquity UPLC BEH300 C18 column (1.7 μm , 2.1 mm ID \times 150 mm L, Waters). Peptide elutions were performed at a flow rate of 0.4 mL/min with a 10-70% gradient of buffers B/A over 10 min (solvent A composition: H_2O /formic acid, 99.9/0.1 (v/v) and solvent B composition: ACN/formic acid, 99.9/0.1 (v/v)). The eluted solution was directly injected into the coupled MS system. Acquisition and analysis of the peptide samples were carried out in the positive mode, within a mass range of m/z 100-2,000 using the Agilent MassLynx software version 4.1 (Waters). The mass spectrometer settings for the MS analyses were: capillary voltage, 0.5 kV; cone voltage, 40 V; source temperature, 150°C; desolvation temperature, 600°C; gas flow, 80 L/hr; and gas desolvation, 1000 L/hr. MS data were acquired using a data-dependent acquisition method (DDA) for which MS/MS data were acquired using CID activation mode based on mass and charge state of the candidate ions. For calibration, an external lock mass was used with a separate reference spray (LockSpray) using a solution of leucine enkephalin eluted at a flow rate of 5 $\mu\text{L}/\text{min}$. The calibration was based on the MS detection of m/z 278.1141 and 556.2771 ions at collision energy of 23 eV. The resulting MS/MS spectra data were analysed by *De Novo* sequencing using PEAKS® studio version 5.2 software (Bioinformatics Solutions Inc.) with the following settings: trypsin or V8 protease; carbamidomethyl (C) as a fixed modification and amidation as variable modification; mass accuracy for MS/MS data at 0.05 Da; and mass accuracy for the precursor mass at 20 ppm. Amino acid sequence scores between 50 and 100 were recorded.

Amino acid sequence determination based on Edman degradation was performed using an Applied Biosystems gas-phase sequencer model 492 (s/n: 9510287J). Phenylthiohydantoin amino acid derivatives generated at each sequence cycle were identified and quantitated on-line with an Applied Biosystems Model 140C HPLC system using the data analysis system for protein sequencing from Applied Biosystems (software Procise PC v2.1). The PTH-amino acid standard kit (Perkin-Elmer P/N 4340968) was used and reconstituted according to the manufacturer's instructions. The procedures and reagents used were those recommended by the manufacturer. Chromatography was used to identify and quantify the derivatized amino acid removed at each sequence cycle. Retention times and integration values of peaks were compared to the chromatographic profile obtained for a standard mixture of derivatized amino acids.

Automated patch-clamp recordings. For primary screening, planar assay electrophysiology recordings were made on an IonWorks Quattro® system (Molecular Devices, Sunnyvale, CA, USA) enabling population patch-clamp (PPC) measurement. HEK-293 cell suspensions were prepared as described in a previous article using similar technology (Chambard *et al.*, 2014). For electrophysiological recordings, cells were resuspended in 5 mL pre-filtered external buffer containing (in mM): 137 NaCl, 4 KCl, 1 MgCl_2 , 1.8 CaCl_2 , 10 HEPES, 5 glucose (osmolarity set at 306 mOsm/L and pH 7.3 adjusted with NaOH). All recordings were made using an internal solution containing (in mM): 100 K-gluconate, 40 KCl, 1 MgCl_2 , 1 EGTA, 5 glucose and 10 HEPES (osmolarity set at 300 mOsm/L and pH 7.4 adjusted with KOH). Sealing process and access of the perforated patch-clamp configuration were obtained as already described in the literature (Trivedi *et al.*, 2008). Cells/wells were clamped using the electronics (E-) head held at -120 mV (with reference to a common "intracellular" ground electrode). Pre-compound currents were recorded, followed by addition of test peptide venoms prepared in external solution complemented with 0.2% bovine serum albumin (BSA; Sigma). Fractions were incubated for 10 min before the post-compound response was recorded. The

pre- and post-compound responses were evoked by a voltage train as follows: after a 10-sec period holding at -120 mV, ten pulses, each consisting of a 50-ms step to the voltage of the peak current of the current-voltage relationship for each channel, were applied at 10 Hz (50-ms interpulse interval). The current signal was sampled at 10 kHz. Currents were leak-subtracted based on the estimate of current evoked during the -10 mV step at the start of the voltage pulse protocol. Pre- and post-compound sodium current amplitudes were measured automatically from the leak-subtracted traces by the IonWorks software through averaging a 10 ms current during the initial holding period at -90 mV (baseline current) and subtracting this from the peak of the current response for each of the eight voltage steps. Data shown are calculated for pulse 1 (tonic block) or pulse 10 (use-dependent block). Filters were set to a pre-scan seal resistance of 40 M Ω , pre-scan hNa_v1.7 current amplitude of 200 pA, and post-scan seal resistance of 40 M Ω . Cells that did not meet these criteria were discarded from the measurements. Dividing the post-scan current amplitude by the respective pre-scan current amplitude for each well assessed the degree of inhibition of the hNa_v1.7 current.

Secondary screening for hit confirmation, as well as rapid selectivity check, were also performed on an automated patch-clamp system, the QPatch HTX (Sophion Bioscience, Denmark) recording currents in whole-cell configuration, allowing both signal acquisition and data analyses (Bell *et al.*, 2018). The day of their use, HEK-293, CHO and U2OS cells were transferred into Eppendorf tubes containing a FreeStyle 293 expression medium (Gibco) which were then placed in the automated electrophysiology platform. The extracellular medium composition for hNa_v-overexpressing HEK-293 cells was (in mM): NaCl 154, KCl 4, CaCl₂ 2, MgCl₂ 1, and HEPES 10 (pH 7.4, adjusted with NaOH), and that of intracellular (*i.e.*, patch-clamp pipette) medium: CsF 150, EGTA/CsOH 1/50, HEPES 10, NaCl 10, MgCl₂ 1, and CaCl₂ 1 (pH 7.4, adjusted with CsOH). The extracellular medium composition for hCa_v-overexpressing CHO cells was (in mM): NaCl 145, KCl 4, CaCl₂ 10, and HEPES 10 (pH 7.4, adjusted with NaOH), and that of intracellular medium: CsF 27, CsCl 112, EGTA 8.2, HEPES 10, NaCl 2, and MgATP 4 (pH 7.4, adjusted with CsOH). The extracellular medium composition for hK_v-overexpressing CHO and U2OS cells was (in mM): NaCl 145, KCl 4, CaCl₂ 2, MgCl₂ 1, HEPES 10, and D-glucose 10 (pH 7.4, adjusted with NaOH). That of intracellular medium was (in mM): KCl 120, CaCl₂ 5.4, EGTA 10, HEPES 10, Mg-ATP 4, and MgCl₂ 1.75 (pH 7.4, adjusted with KOH) for hK_v11.1-overexpressing CHO cells; K aspartate 130, EGTA 5, HEPES 10, and MgCl₂ 5 (pH 7.4, adjusted with KOH) for hK_v1.5-overexpressing CHO cells; K fluoride 120, KCl 20, EGTA/KOH 10/31.25, EDTA 10, and HEPES 10 (pH 7.2, adjusted with KOH) for hK_v7.1-overexpressing U2OS cells; and KCl 120, CaCl₂ 5, EGTA 10, HEPES 10, and MgCl₂ 1.75 (pH 7.4, adjusted with KOH) and 1.75 mM MgCl₂ (pH 7.4 adjusted with KOH) for hKir2.1-overexpressing CHO cells. Venom fractions and sub-fractions, as well as CyrTx-1a, were diluted in the extracellular medium supplemented with bovine serum albumin (0.1%), to give the final concentrations indicated in the text. The times of incubation varied between ~2 and ~7 min to achieve steady-state effects. The experiments were carried out at room temperature (20-22°C). The hNa_v-overexpressing HEK-293 cells were maintained at a holding potential of either -90 mV (hNa_v1.5) or -100 mV (other hNa_v channel subtypes). Currents were elicited at a frequency of 0.2 Hz (at least 4.78-s interpulse interval) by 20-ms test-pulses to -20 mV (hNa_v1.1, 1.2, 1.4, and 1.7), -10 mV (hNa_v1.3), -40 mV (hNa_v1.5), -15 mV (hNa_v1.6) or +10 mV (hNa_v1.8), preceded by 200-ms (hNa_v1.5) or 40-ms (hNa_v1.7) pulses to -120 mV, or not (hNa_v1.1, 1.2, 1.3, 1.4 and 1.6). The hCa_v-overexpressing CHO cells were maintained at a holding potential of -50 mV (hCa_v1.2) or -100 mV (hCa_v3.1 and 3.2), and currents were elicited at a frequency of 0.05 Hz (at least 19.5-s interpulse interval) by 200-ms test-pulses to +0 mV (hCa_v1.2) or by 500-ms test-pulses to -20 mV (hCa_v3.1 and 3.2). The hK_v11.1-overexpressing CHO cells were maintained at a holding potential of -80 mV, and tail currents were elicited at a frequency of 0.07 Hz (4.47-s interpulse interval) by 5-sec test-pulses to -50 mV, preceded by 4.8-sec pulses to +20 mV following 20-ms pulses

to -50 mV. The hK_v7.1-overexpressing U2OS cells were maintained at a holding potential of -60 mV, and currents were elicited at a frequency of 0.07 Hz (13.08-s interpulse interval) by 1-sec test-pulses to 40 mV preceded by 200-ms pulses to -80 mV. The hKir2.1-overexpressing CHO cells were maintained at a holding potential of -20 mV, and currents were elicited at a frequency of 0.03 Hz (31.83-s interpulse interval) by 500-ms pulses to -120 mV followed by 1-sec potential ramps from -120 to 0 mV. The leakage current was not compensated for. The concentration-response relationships were established by expressing the peak amplitude of the sum of ten cell currents recorded after 2-7 min in the presence of a given toxin concentration relatively to that of the sum of these currents recorded before toxin incubation.

Manual patch-clamp recordings. A few days before experiments, HEK-293 cells were transferred to 12-mm glass coverslips placed in 35-mm Petri dishes. The day of their use, the culture medium was changed to a standard physiological medium of the following composition (in mM): NaCl 134, KCl 3, CaCl₂ 1, MgCl₂ 1, D-glucose 10, tetraethylammonium chloride 10, CdCl₂ 0.1, and N-2-hydroxyethylpiperazine-N'-2-ethanesulfonic acid (HEPES) 10 (pH 7.35, adjusted with NaOH), for a minimum of 15 min at 37°C prior to recordings. The day of their use, the DRG neurons plated on coverslips were transferred, for a minimum of 30 min at 37°C prior to recordings, in 35-mm Petri dishes filled with a standard physiological medium similar to that used for HEK-293 cells. The HEK-293 cells or DRG neurons, plated on coverslips, were then transferred in the recording bath filled with the standard physiological medium.

Whole-cell manual patch-clamp experiments were performed by using a MultiClamp 700B integrating patch-clamp amplifier and the pClamp10.6 software (Molecular Devices), as previously described (Gonçalves *et al.*, 2018). The patch-clamp pipettes were filled with a medium composed of (in mM): CsCl 90, CsMeSO₃ 40, NaCl 10, MgCl₂ 2, EGTA 2, Na₂ATP 4, and HEPES 10 (pH 7.32, adjusted with CsOH), and had ~3-MΩ resistance in the standard physiological medium. A fast solution application system allowed changing the solution (standard physiological medium supplemented or not with a given toxin concentration) around the recorded cell or neuron within a few seconds. The experiments were carried out at constant room temperature (22°C).

The cells and neurons were maintained at a holding potential of -60 mV, and currents were elicited at a frequency of 0.5 Hz (0.95-s interpulse interval) by 50-ms test-pulses to -20 mV preceded by 1-sec pulses to -120 mV. The concentration-response relationships were established by expressing the peak current amplitude measured in the presence of a given toxin concentration relatively to that before toxin application. Current-voltage relationships were obtained by varying test-pulses from -80 to +10 mV in 5-mV increments, and steady-state inactivation-voltage relationships by changing pre-pulses from -120 to -20 mV in 5-mV increments.

References

- Bell DC, Dallas ML (2018). Using automated patch clamp electrophysiology platforms in pain-related ion channel research: insights from industry and academia. *British journal of pharmacology* 175: 2312-2321.
- Chambard JM, Tagat E, Boudeau P, Partiseti M (2014). Transforming TRP channel drug discovery using medium-throughput electrophysiological assays. *J. Biomol. Screen* 19: 468-477.
- Gonçalves TC, Boukaiba R, Molgo J, Amar M, Partiseti M, Servent D, *et al.* (2018). Direct evidence for high affinity blockade of NaV1.6 channel subtype by huwentoxin-IV spider peptide, using multiscale functional approaches. *Neuropharmacology* 133: 404-414.
- Trivedi S, Dekermendjian K, Julien R, Huang J, Lund PE, Krupp J, *et al.* (2008). Cellular HTS assays for pharmacological characterization of Na(V)1.7 modulators. *Assay Drug Dev. Technol.* 6: 167-179.